NASA CR-111867

# AN ANALYSIS OF CORRELATING PARAMETERS RELATING TO HOT-GAS INGESTION CHARACTERISTICS OF JET VTOL AIRCRAFT

by V. Krishnamoorthy



March, 1971

Prepared Under Contract No. NAS1-10448 by

Bell Aerospace Company
Buffalo, New York

for

NATIONAL AERONAUTICS AND SPACE ADMINISTRATION

## ABSTRACT

Inlet-air temperature rise data obtained from previous tests on two small-scale configurations of a jet VTOL fighter-type model over a range of exhaust pressure ratios, exhaust gas temperatures and surface wind velocities, is analyzed for correlation with several correlating parameters. The correlating parameters are used to predict the large-scale model inlet temperature rise and the large and small-scale results are compared.

CONTENTS

# AN ANALYSIS OF CORRELATING PARAMETERS RELATING TO HOT-GAS INGESTION CHARACTERISTICS OF JET VTOL AIRCRAFT

By V. Krishnamoorthy
Bell Aerospace Company

## SUMMARY

Small-scale inlet temperature rise (ITR) data obtained previously at the Bell Aerospace Company's Jet Impingement Test Facility is analyzed for correlation with several correlating parameters. These ITR data were obtained for two 0.24 scale configurations of a generalized jet VTOL fighter-type model for a range of exhaust total temperatures (900°F to 1400°F) and exhaust total pressure ratios (1.1 to 2.0) at various wind velocities (0 to 55 ft/sec).

The ITR data of the side inlets configuration correlated well with the jet Reynolds number at low wind speeds. At high wind speeds the jet exit dynamic pressure, momentum and kinetic energy gave good correlation. For the top inlets configuration, a buoyancy parameter is used for correlation of ITR at all wind speeds.

The small-scale data were compared with data measured by NASA, Langley using a larger geometrically similar model, at equal values of these correlating parameters. For the side inlets configuration, good agreement between the small and large-scale ITR data was found at low speeds only when comparison was made at equal Reynolds number.

Comparison of small and large-scale ITR of the top inlets configuration, based on equal buoyancy conditions or equal exhaust velocity and temperature conditions was found to be poor.

# INTRODUCTION

Hot-gas ingestion represents a serious problem in the design of jet VTOL aircraft. Inlet-air temperature rise (ITR) of more than 200°F has been observed for typical jet lift configurations operating near the ground and with surface winds. The severity of the problem becomes clear when the level of ITR is converted into engine thrust loss, which is three to four percent per 10°F inlet temperature rise. Besides mean ITR levels, wide and rapid temperature fluctuations and temperature distribution distortions at the inlet face can cause engine compressor stall. Both large and small-scale model tests have been conducted by various investigators (refs. 1 to 7) to determine ingestion characteristics. These tests have shown that ingestion is highly dependent on configuration such as the inlet and exhaust location, engine arrangement, exhaust incidence, wing size and location, etc. The geometry effects are particularly significant near the ground ($h/D_e < 5$) where h is the vehicle height above ground, and $D_e$ is the equivalent engine nozzle diameter. The exhaust jet conditions and the magnitude and direction of surface winds also have strong influence on the ingestion characteristics.

The effect of model scale on ingestion characteristics has so far been assessed by two different simulation techniques. In the first, referred to as thrust simulation, it is assumed that the flow field near the model and full-scale vehicle are dynamically similar when the jet exit velocity, temperature, inlet velocity, vehicle velocity and wind velocity on the model and full-scale vehicle are identical. The other approach to model testing is buoyancy simulation. This requires that the ratio of inertia to buoyant forces in the hot gas flow between the model and full-scale craft be equal. Further the ratio of inlet to exit dynamic pressure should be the same for model and full-scale craft. The jet exhaust temperature rise above the ambient level for the model should be proportional to the full-scale value. When relative wind is present, the ratio of free stream to jet exit dynamic pressure should be the same for the model and full-scale vehicle. It is assumed that, when these conditions are met, the flow fields are dynamically similar.

The scale effect has been evaluated from model tests incorporating these two approaches. Abbott (ref. 8) using a 1/10th scale moving model of H.S. 1127 aircraft, conducted tests to determine intake temperature rise using buoyancy simulation. The model ITR when compared with the full-scale results showed fair agreement. Tests using thrust simulation conditions (refs. 6 and 7) have led to contrary conclusions. Based on the test results of a full-scale lift engine pod with two engines and the corresponding scale model, it was concluded in reference 6 that the overall flow field and hot-gas ingestion are scalable. However, ingestion data (ref. 7) of two configurations of a fighter-type jet VTOL model featuring four lift jets in the fuselage when compared with the results (ref. 3) of a four times larger model showed poor agreement. These results indicate that the correct procedure for small-scale tests is not well established.

The object of this investigation is to determine empirically the scaling parameters which must be maintained when conducting small-scale tests. For the purpose of analysis, available data from references 7 and 9 are used. These ITR data were

obtained for two 0.24 scale configurations of a NASA jet VTOL fighter-type model for a range of exhaust total temperatures (900°F to 1400°F) and exhaust total pressure ratios (1.1 to 2.0) at various wind velocities (0 to 55 ft/sec). For the zero wind ($V_\infty = 0$) case, the far field contribution to inlet temperature rise is assumed to be small and the correlating parameters pertaining to the near field are found for both the side and top inlet configurations. The correlating parameters at finite wind velocities and over the range of tested exhaust conditions are then determined for both model configurations.

These correlating parameters are then used to predict the large scale ITR at zero and finite wind speeds for both model configurations and the large and small scale results are compared and discussed.

## SYMBOLS

| | |
|---|---|
| $C_{p,\,j}$ | specific heat at constant pressure of the exhaust gas, ft-lb/lb mass (°F) |
| $D_e$ | equivalent nozzle diameter (diameter of a circle whose area is equal to the sum of the areas of the individual nozzles), ft |
| $D_j$ | nozzle exit diameter, ft |
| g | gravitational acceleration, $ft/sec^2$ |
| h | nozzle exit height above ground plane, ft |
| ITR | inlet-air temperature rise (final inlet-air temperature minus initial ambient temperature), °F |
| $m_j$ | total mass flow at the nozzle exit, lb-sec/ft |
| $p_\infty$ | ambient static pressure, $lb/ft^2$ |
| $P_j$ | nozzle exit total pressure, $lb/ft^2$ |
| $q_\infty$ | free stream dynamic pressure, $lb/ft^2$ |
| $q_j$ | jet exit dynamic pressure, $lb/ft^2$ |
| $(q_\infty / q_j)^{\frac{1}{2}}$ | effective velocity ratio |
| R* | radius of ground jet separation point, ft |
| $S_j$ | total jet nozzle area, $ft^2$ |

| | |
|---|---|
| $S_w$ | wing area, $ft^2$ |
| $T_\infty$ | ambient temperature, °F |
| $T_i$ | inlet-air temperature, °F |
| $T_j$ | nozzle exit total temperature, °F |
| $V_\infty$ | free stream velocity, ft/sec |
| $V_j$ | nozzle jet exit velocity, ft/sec |
| $\rho_\infty$ | ambient air density, lb $sec^2/ft^4$ |
| $\rho_j$ | nozzle exit gas density, lb $sec^2/ft^4$ |
| $\mu_j$ | dynamic viscosity of gas at nozzle exit, lb $sec/ft^2$ |
| $\beta$ | coefficient of thermal expansion of gas (reciprocal of ambient temperature), $°F^{-1}$ |
| $\psi$ | wind heading (azimuth) angle, degrees |

## TEST FACILITY, MODEL, AND INSTRUMENTATION

### Test Facility

The data used in the present analysis were obtained at the Bell Aerospace Company's Jet Impingement Test Facility. The facility is of the outdoor type and it provides variable hot gas exhaust flows with exit total pressure ratios from 1.1 to 2.0 and exhaust total temperatures from 500°F to 1700°F with a maximum exhaust flow rate of 2.8 lb/sec.

The main ground plane of the facility is rectangular, smooth and level to a radial distance of 13 ft (approximately 49 equivalent diameters). An auxiliary ground plane (10 ft by 8 ft) scaled to the dimensions of the test section platform of the NASA Langley Research Center full-scale wind tunnel was placed about 12 inches above the main ground plane. The model and flow system components were supported by a single hydraulic cylinder mounted on the super structure. This allowed the model height to be varied up to 4 ft and provided unobstructed space for overall flow field development.

A wind machine with 6 x 10 ft exit section was used to produce relative wind speeds up to 55 ft/sec at various directions ( $\psi$ ) to the model.

Detailed description of the test facility is given in reference 7.

### Model

Two 0.24 scale model configurations (side inlets and top inlets) of the NASA model described in reference 3 were used. Both configurations had four exhausts located in the fuselage in a rectangular arrangement, and a high delta wing with a wing area to jet nozzle area ratio, $S_W / S_j$, of 43. The exhaust jet arrangement had four 1.49 inch diameter convergent nozzles, or an equivalent jet diameter, $D_e$, of 0.248 ft. The top inlet arrangement consisted of four 1.92 inch diameter inlets. The two side inlets were approximately rectangular in cross section, the area of each being 5.88 sq. in. The schematic arrangement of the two model configurations is given in reference 7.

Tests were conducted with the model at constant height above ground of $h/D_e$ = 1.2 and 3.0 for the side and top inlet configurations, respectively.

### Instrumentation

The inlet-air temperature data and the wind conditions were recorded in the form of time histories by using oscillograph recorders. The jet exhaust conditions were measured by total temperature and pressure probes. Detailed description of the instruments, their locations with respect to the model and their accuracies are found in reference 7.

## RESULTS AND DISCUSSION

Basic inlet temperature rise data of the small-scale side and top inlet configurations are presented first. Results of the correlation of ITR with several candidate correlating parameters are then discussed. Finally, the inlet temperature rise of the small scale is compared with the ITR of the large scale based on these correlating parameters.

### Basic Small-Scale Data

Side Inlets. - The variation of ITR above ambient ($T_i - T_\infty$) with jet exit total pressure ratio ($P_j / p_\infty$), exit total temperature ($T_j$), and with surface head wind velocity ($V_\infty$) is shown in figure 1. The overall flow field is assumed to be symmetrical with respect to the inlets and the ITR at inlets 1 and 2 is averaged. The inlet temperature rise generally increases with increase in pressure ratio and temperature for all $V_\infty$. For a fixed pressure ratio and temperature, the effect of increasing wind speed is to increase the ITR level to a maximum value and then to lower it at higher speeds. This maximum value and the $V_\infty$ corresponding to it increase with increasing pressure ratio.

These results can be interpreted in the light of the general discussions of the mechanism of hot-gas ingestion presented in (refs. 1 to 7, and 10 to 15). The schematic representation of the recirculating flow field with head wind is reproduced here from reference 7, in figure 2. In still-air ($V_\infty = 0$), the jet efflux from the present multi-jet exhaust arrangement, after striking the ground, forms an upwash or fountain of exhaust gas flowing upward between the main jet streams. This upwash spreads outward along the bottom of the craft, flows upward around the fuselage and is sucked into the inlets with very little time to cool by mixing with the ambient air. Increase in exit pressure ratio and temperature causes increase in the momentum and heat content of the upwash flow, resulting in increased ITR levels. It appears that when $V_\infty$ is zero the dominant contribution to ITR arises from the near field upwash flow and the contribution from the recirculation of the far field flow is quite small.

For finite wind speeds, ITR is governed both by the near and far field flows. With surface winds the far field hot gases are blown back toward the model. For a fixed inlet and nozzle location, the ground jet separation and recirculation of the far field flow depend primarily on the free stream to jet dynamic pressure ratio (ref. 14). For a fixed exhaust pressure ratio and at low wind speeds, separation occurs farther from the jet centerline and the far field gases are blown back over the top of the model. When the wind speed is increased, the separation line moves closer to the model, resulting in direct ingestion by the inlets. At high wind speeds the recirculating flow is blown under the inlets causing reduced ingestion. In the near field, the oncoming wind also alters the upwash flow characteristics (ref. 12) and depending on the wind velocity changes the ingestion levels.

Top Inlets. - The variation of ITR with exhaust pressure ratio and temperature at various head wind velocities is shown in figure 3. Again assuming flow symmetry, the averages of ITR at inlets 1 and 2 and at inlets 3 and 4 are shown. At low wind speeds ($V_\infty \leq 20$ fps), the inlet temperature rise decreases with increasing pressure ratio followed by an increase in ITR with increasing $P_j / p_\infty$ at higher speeds. It is seen that the inlets 1 and 2 are more prone to high ingestion levels than inlets 3 and 4. Unlike the side inlets, the general levels of ITR are markedly low for the top inlets for all wind speeds. The reason is that the inlets lie on top of the wing and the upwash generated by the exhaust jets is largely blocked by the wing, thereby greatly suppressing the near field ingestion into the inlets. The inlet temperature rise therefore appears to arise mainly from the far field recirculating hot-gas flow resulting in reduced ingestion levels compared to the side inlets.

## Correlation of ITR With Selected Correlating Parameters

Significance of Selected Correlating Parameters.- The scaling parameters applicable to the flow fields generated by the present model configuration may be obtained from dimensional analysis and from balancing of momentum and heat transport in the overall flow field. Of the many correlating parameters that are possible with the chosen flow variables, the following which are deemed to be significant were examined in the analysis: Reynolds number, Eckert number, jet exit dynamic pressure, exit momentum, kinetic energy and effective velocity ratio (square root of the ratio of free stream dynamic pressure to jet dynamic pressure).

The buoyancy parameter represents the ratio of inertia forces to buoyant forces in the flow. In the free jet region of the exhaust flow and near the origin of the ground jet, buoyancy forces are secondary to jet momentum forces. However, farther from the jet center (far field) the buoyancy forces may become important depending on the external winds. In the no-wind condition, the radial ground jet dynamic pressure decays more rapidly than the corresponding differential temperature and at some point along the ground the buoyancy forces counteract the radial momentum and shear forces at the ground, thereby causing flow separation. The separation of the ground jet and the ensuing recirculation by free convection of the far field gases depend on the buoyancy parameter as shown by Cox in reference 13. At low wind speeds the buoyancy forces in the far field may still be comparable to the momentum and shear forces in the ground jet, and the opposing free stream dynamic pressure forces. With increasing wind speed it would appear that the buoyancy forces become less effective and the ground jet separation and recirculation are governed primarily by dynamic pressure forces.

The jet Reynolds number represents the ratio of inertia to viscous forces in the exhaust flow. In flow phenomena involving forced convection, the heat transfer depends on Reynolds number and Prandtl number (ref. 16). Prandtl number depends on the physical properties of the exhaust gases and is nearly unity for the present tests. In the near field of the jets, the upwash develops into a three-dimensional, turbulent free-

shear flow. Limited quantitative results are available (refs. 12, 17, and 18) regarding upwash characteristics and from these it is inferred that for the present configuration and tests, the upwash has appreciable velocity and temperature. Therefore, heat transfer to the inlets from the near field is expected to occur by forced convection as opposed to natural convection.

The Eckert number (ref. 16) denotes the ratio of kinetic energy of the issuing jet to the heat lost by exhaust gases. This parameter is examined for correlation of ITR, where the ingestion is dominated by the near field.

The jet exit momentum, dynamic pressure and kinetic energy in turn affect the momentum flux and the energy transport in the upwash, radial ground jet and in the recirculating flow. Correlation of ITR with these parameters is investigated.

The effective velocity ratio is found by Abbott (ref. 14) to be an important parameter in correlating the upstream separation criterion for a radial ground jet in a cross wind. Abbott's results pertain to single and twin nozzles operating at low exhaust pressure ratios and temperatures. It is found that the separation point from the jet centerline is fixed uniquely for a fixed velocity ratio and at the point of separation the free stream velocity is about half the local maximum velocity of the ground jet. The same conclusion is reached in reference 7, where the measurements were made with four jets operating at high $P_j / p_\infty$ and $T_j$. Abbott also found (ref. 14) that the separation point could be correlated with the height of the recirculating flow. Since the separation criteria and the height of the recirculating flow correlate well with the effective velocity ratio, this parameter was investigated for ITR correlation.

## ITR Correlation

Side Inlets. - The inlet temperature rise above ambient, $T_i - T_\infty$, is normalized with respect to the jet excess temperature, $T_j - T_\infty$. Correlation of normalized ITR with jet Reynolds number is shown in figure 4. The test values correspond to a wide range of jet exhaust conditions at two wind speeds. The accuracy of data plotted along the ordinate is from $\pm 0.003$ to $\pm 0.006$, the lowest variance being associated with $T_j = 1400^\circ F$ data and the highest with $T_j = 900^\circ F$ data. It appears that good correlation exists for $V_\infty = 0$ and 19.6 ft/sec, since the majority of the data lie within the accuracy bands. It is seen that the temperature ratio increases with increasing Reynolds number and wind speed. The data for wind velocities greater than about 20 ft/sec are not shown in the figure since the exhaust temperature showed as an independent parameter indicating that correlation was not achieved.

The correlation of $(T_i - T_\infty / T_j - T_\infty)$ with modified Eckert number, $[V_j^2 / g C_{p,j} (T_j - T_\infty)] (T_\infty / T_j)$, is presented in figure 5. This parameter is obtained by multiplying the Eckert number and temperature ratio $(T_\infty / T_j)$. Correlation again exists only for $V_\infty = 0$ and 19.6 ft/sec and the ITR variation is similar to that of Reynolds number.

The correlations of normalized ITR with jet exit dynamic pressure, momentum and kinetic energy were achieved only at higher wind velocities ($V_\infty \geq 30$ ft/sec) and these are shown in figures 6, 7, and 8 respectively. The variation of $(T_i - T_\infty / T_j - T_\infty)$ with each of these parameters appears to be similar and this may be expected since the kinetic forces in the flow are common to each. It is seen that the temperature ratio increases when the wind speed is reduced or when the value of the parameter is increased.

The correlation of $(T_i - T_\infty / T_j - T_\infty)$ with modified Cox number, $[V_j^2 / g D_e (T_j - T_\infty / T_\infty)] (T_j / T_\infty)$, is presented in figure 9. Cox (ref. 13) has shown that a suitable parameter for correlating experimental data on a single jet case is $[V_j^2 / g D_e \beta (T_j - T_\infty)] (T_\infty / T_j)^{1/2}$ where $\beta$, the coefficient of thermal expansion of the exhaust gas is assumed to be $1/T_\infty$. For the present multi-jet case, it was found that inclusion of temperature ratio $(T_j / T_\infty)$ instead of $(T_\infty / T_j)^{1/2}$ improved the correlation of data. It is noted that the ITR variation with modified Cox number is similar to those shown in figures 6 to 8. This suggests that the buoyancy forces in the flow are secondary in importance to the kinetic forces for wind velocities exceeding 30 ft/sec.

The variation of $(T_i - T_\infty / T_j - T_\infty)$ with effective velocity ratio, $(q_\infty / q_j)^{1/2}$ is shown in figure 10. It is seen that correlation is poor since $V_\infty$ appears as an independent parameter. It is interesting to note that the curves shift systematically to the right with increasing wind speed. For a specified velocity ratio, the ground jet separation point and the height of the recirculating flow are fixed (ref. 14) and yet the temperature ratio appears to increase with increasing wind speed. The reason for this may be that as $V_\infty$ is increased, the hot gases will arrive at the inlets sooner for a fixed recirculating flow path length. The mixing time, therefore, will be reduced and consequently $(T_i - T_\infty)$ will be raised. Further tests are needed to confirm whether the recirculating flow envelope is uniquely determined for a specified $(q_\infty / q_j)^{1/2}$.

Top Inlets. - The correlating parameters used for the side inlets were applied to the top inlet ITR data for correlation and none of them appeared to be satisfactory. The modified Cox number was finally selected since it gave minimum data scatter compared to the other parameters. Correlation curves of normalized ITR with modified Cox number are shown in figures 11 and 12 corresponding to ITR average of inlets 1, 2 and inlets 3, 4 respectively.

## Comparison of Small and Large-Scale ITR

In order to compare correctly the small and large-scale ITR data at equal values of the selected correlating parameter, it is necessary to know the true exhaust conditions of the small and large-scale models. The exhaust conditions of the small-scale model were controlled and accurately measured. The large-scale model was powered by a turbojet engine and all the tests were conducted at a nominal exhaust pressure ratio of 1.8 and temperature of 1200°F. The actual pressure ratio varied with the inlet temperature rise in a manner characteristic of jet engines. The variation of

corrected exhaust pressure ratio with ITR for the side and top inlets of the large-scale model is found in reference 7.

Side Inlets. - Comparison of small and large scale $(T_i - T_\infty / T_j - T_\infty)$ at equal Reynolds number is presented in figure 13 for the side inlets. Comparison is made only for $V_\infty = 0$ and 20 ft/sec, since data correlation was achieved for these wind speeds only. (See fig. 4.) The small-scale data in figure 13 correspond to the median curves shown in figure 4. The maximum value of the Reynolds number of small-scale tests is only $5 \times 10^5$ and the large-scale temperature ratio at $V_\infty = 0$ and 20 ft/sec is therefore predicted by extrapolation. The predicted temperature ratios agree closely with the large-scale test values.

Comparison of small and large scale ITR based on equal modified Eckert number (not shown) was found to be inferior to equal Reynolds number condition.

Small to large-scale comparison at equal jet exit dynamic pressures, is shown in figure 14. Comparison is made at $V_\infty = 30$ ft/sec and beyond since small-scale data correlation was achieved only at those speeds. It is seen that considerable variation in ITR levels exists between the model and the large scale.

Jet exit momentum and kinetic energy comparisons are shown in figures 15 and 16, respectively. The small-scale normalized ITR increases with increasing momentum and kinetic energy values. The maximum value of the momentum or kinetic energy of the small-scale model differs approximately by a factor of 1/16 (corresponding to small scale to large scale jet area ratio) from the large-scale test values. Because of this large difference, prediction of large-scale $(T_i - T_\infty / T_j - T_\infty)$ by extrapolation of small-scale data is made difficult. It is noted that the large-scale model has significantly lower ingestion levels than the small-scale, especially at $V_\infty = 40$ and 50 ft/sec.

It would be of interest to know how the small-scale $(T_i - T_\infty / T_j - T_\infty)$ would vary with further increase in momentum or kinetic energy from the present maximum test values. For a given $T_j$, the jet exit velocity, $V_j$, increases when $P_j / p_\infty$ is increased up to the critical value. Beyond the critical pressure ratio, increase in $V_j$ is possible only by raising $T_j$ and $V_j$ varies in proportion to the square root of the jet total temperature. It can be shown that the jet mass flow is proportional to $P_j / (T_j)^{1/2}$. Hence for a given nozzle area the jet momentum can be further increased by increasing the $P_j$ and is independent of $T_j$. Similarly the jet kinetic energy increases when $P_j$ and $T_j$ are raised. For a fixed $V_\infty$, increase in momentum flux or kinetic energy of the jet moves the separation point of the ground jet farther from the jet center line resulting in a dimunition of hot-gas ingestion due to the far field. However, the ingestion due to the near field flow may increase when the jet momentum flux or kinetic energy is increased. It is difficult to determine from the present data whether the near or far field ingestion is dominant and further tests are necessary to measure separately the ITR due to fountain and far field at various exhaust conditions and wind speeds.

Finally, the large and small-scale data are compared at equal $V_j$ , $T_j$ conditions in figure 17. It is seen that the comparison is poor.

Top Inlets. - The modified Cox number is selected as the correlating parameter for the top inlets. The model and large-scale data are compared in figure 18 at equal values of this parameter. Since Cox number values of the large-scale tests were smaller than the model, the model data shown in figures 11 and 12 were extrapolated. The small-scale model wind speeds were scaled to equal the effective velocity ratio, $(q_\infty/q_j)^{1/2}$ of the large-scale. This means that for the present tests the model wind speed should be approximately half the large-scale wind speed when inlet temperature rise comparison is made.

The ingestion levels of the model differ significantly from those of large-scale. At low wind speeds, ingestion is low at inlets 1 and 2 of the small-scale model since the upwash is presumably blocked by the wing. However, ingestion is quite high for the large-scale model and the reason for this is not clear. As for inlets 3 and 4, the large-scale ITR is again appreciably higher than that of the model.

Model and large-scale ITR data based on equal $V_j$ , $T_j$ conditions also show poor agreement as illustrated in figure 19.

## CONCLUDING REMARKS

Small-scale inlet temperature rise data obtained from previous tests at the Bell Aerospace Company's Jet Impingement Test Facility were analyzed for correlation with several correlating parameters. It was found that at low head wind velocities ($V_\infty < 20$ ft/sec) the jet Reynolds number correlated the test data well for the side inlets. At high wind speeds ($V_\infty > 30$ ft/sec), good correlation was obtained using jet exit dynamic pressure, momentum and kinetic energy as correlating parameters. Correlation was generally poor for the top inlets, and the buoyancy number, $\left[ V_j^2 / g \beta D_e (T_j - T_\infty) \right] (T_j / T_\infty)$, was used for correlation of ITR at all wind speeds for this configuration.

These correlating parameters were used to compare the small-scale ITR data with the data collected by NASA, Langley using a four times larger geometrically similar model. Comparison of these data at equal Reynolds number was obtained for the side inlets by extrapolation of small-scale data. Close agreement was found between the predicted inlet temperature rise and the large-scale test values. However, the validity of extrapolating the small-scale data needs verification.

Small and large-scale ITR comparisons for the side inlets configuration based on equal dynamic pressure or equal $V_j$, $T_j$ condition was found to be poor.

Neither equal buoyancy parameter nor the equal $V_j$, $T_j$ condition resulted in correlation of large and small-scale ITR for the top inlets.

## REFERENCES


1. Hammond, A. Dudley; and McLemore, H. Clyde.: Hot-Gas Ingestion and Jet Interference Effects for Jet V/STOL Aircraft. Paper presented at AGARD Flight Mechanics Panel Meeting, Gottingen, W. Germany, 1967.

2. McLemore, H. Clyde; and Smith, Charles C., Jr.: Hot-Gas Ingestion Investigation of Large-Scale Jet VTOL Fighter-Type Models. NASA TN D-4609, 1968.

3. McLemore, H. Clyde; Smith, Charles C. Jr.; and Hemeter, Patricia G.: Generalized Hot-Gas Ingestion Investigation of Large-Scale Jet VTOL Fighter-Type Models. NASA TN D-5581, 1969.

4. Hall, Gordon R.: Recirculation and Ingestion Characteristics of a Large-Scale VTOL Lift Engine Pod. NASA CR-72410, 1968.

5. Ryan, Patrick, E.; and Cosgrove, Wayne J.: Empirically Determined Wind and Scale Effects on Hot-Gas Recirculation Characteristics of Jet V/STOL Aircraft. NASA CR-1445, 1969.

6. Hall, Gordon R.: Scaling of VTOL Recirculation Effects. Northrop Norair, NASA Contract NAS3-10498, 1970.

7. Ryan, Patrick E.; and Cosgrove, Wayne J.: The effect of Exhaust Conditions, Surface Winds, and Geometric Scale on Hot-Gas Ingestion for Two Jet VTOL Configurations. NASA CR-66965, 1970.

8. Abbott, W. A.: Estimation of Intake Temperatures During V/STOL Operation From Model Tests. N.G.T.E. Note No. N.T. 600. Min. Aviation (Brit.), 1966.

9. Ryan, Patrick E.; and Cosgrove, Wayne J.: The effect of Exhaust Pressure Ratio, Exhaust Gas Temperature and Wind Velocity on the Inlet Temperature Rise of a Small-Scale Jet VTOL Model - Data Report, Bell Aerospace Company, Report No. 2099-956006, February 1970.

10. Kemp, E.D.G.: Studies of Exhaust Gas Recirculation for VTOL Aircraft. AIAA Paper No. 67-439, July 1967.

11. Harris, A.E.; Marbert, J.A.; and Tatom, J.W.: VTOL Transport Exhaust Gas Ingestion Model Tests. Proceedings of the Seventh Annual National Conference on Environmental Effects on Aircraft and Propulsion Systems, Nav. Air Propulsion Test Center and Inst. Environ. Sci., September 1967, pp. 145-166.

12. Hall, Gordon R., and Rogers, Kenneth H.: Recirculation Effects Produced by a Pair of Heated Jets Impinging on a Ground Plane. NASA CR-1307, 1969.

13. Cox, M.; and Abbott, W.A.: Studies of the Flow Fields Created by Single Vertical Jets Directed Downwards Upon a Horizontal Surface. N.G.T.E. Mem. No. M.390, Min. Aviation (Brit.), 1964.

14. Abbott, W.A.: Studies of Flow Fields Created by Vertical and Inclined Jets When Stationary or Moving Over a Horizontal Surface. C.P. No. 911, Brit. A.R.C., 1967.

15. Kirk, Jerry V.; and Barrack, Jerry P.: Reingestion Characteristics and Inlet Flow Distortion of V/STOL Lift Engine Fighter Configurations. AIAA Paper No. 68-78, January 1968.

16. Schlichting, H.: Boundary Layer Theory. McGraw-Hill Book Co., Inc., 1955.

17. Hertel, H.: Wall Flows and Upstreams Due to the Diversion of Free Jet Groups. NASA TT F-11, 680., 1968.

18. Skifstad, J.G.: Aerodynamics of Jets Pertinent to VTOL Aircraft. Tech Rep. AFAPL-TR-69-28, 1969.

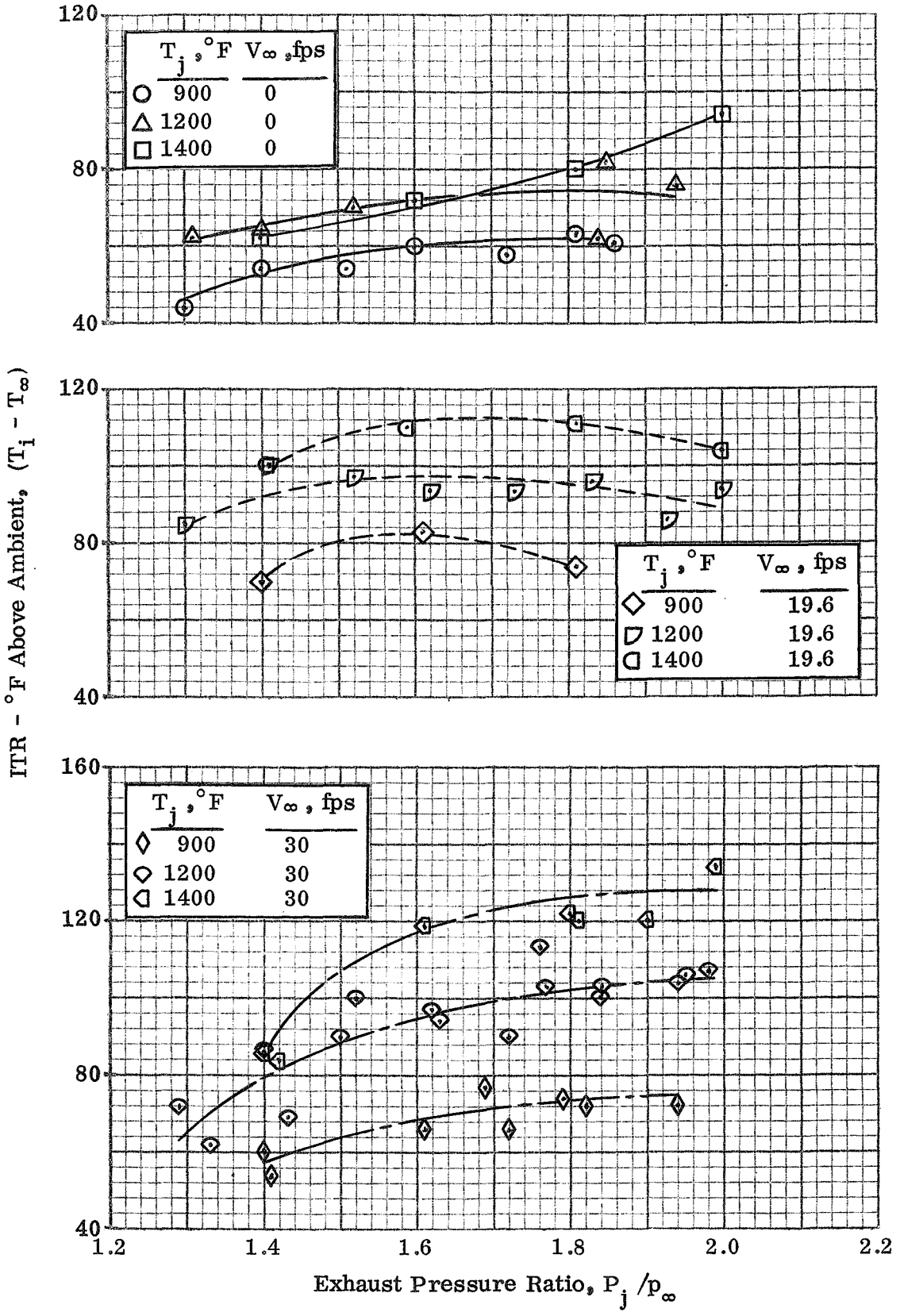


Figure 1. - Variation of ITR With Exhaust Pressure Ratio and Exhaust Temperature at Various Wind Velocities. Side Inlets Configuration, $\psi = 0°$.

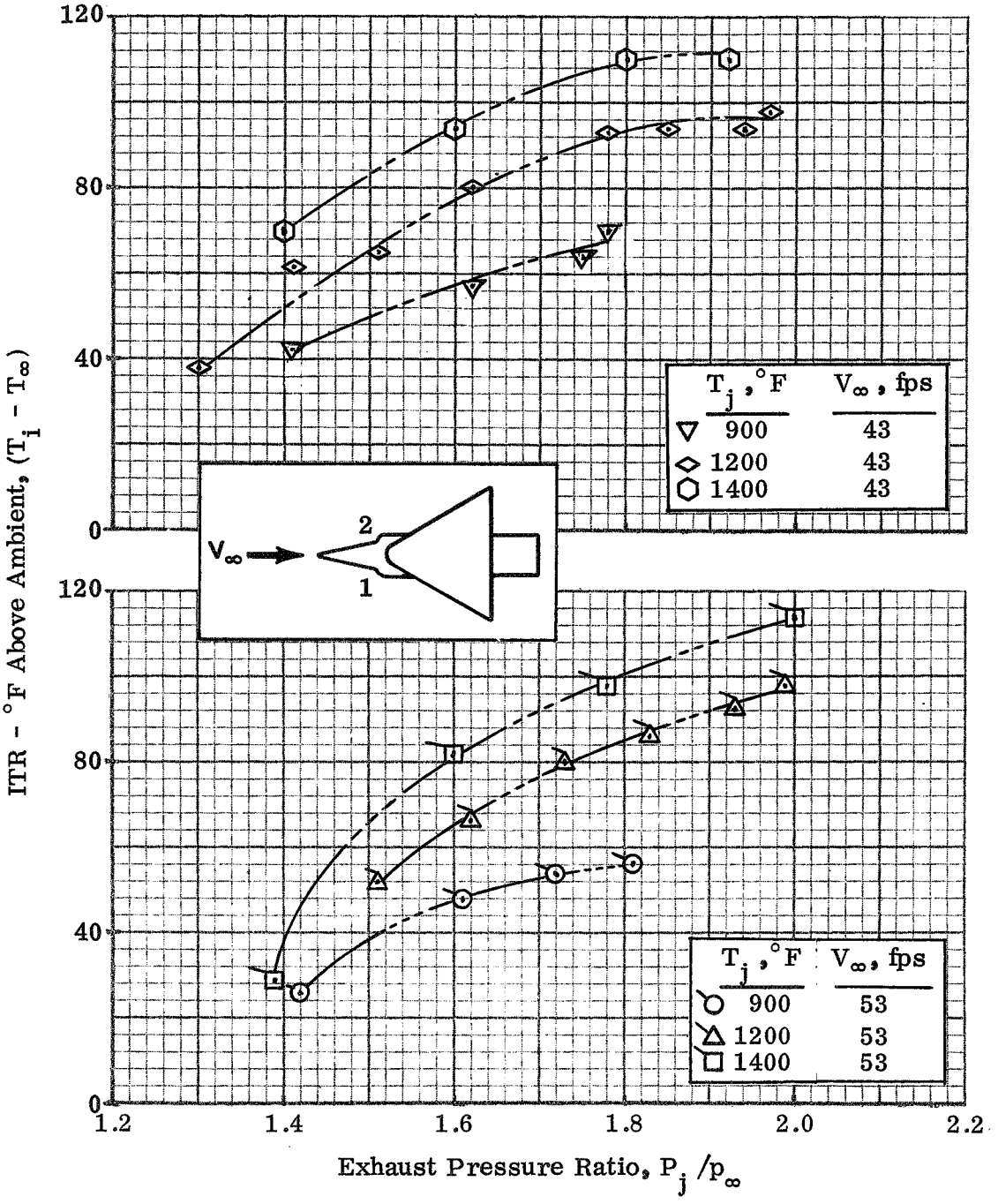


Figure 1. - Concluded.

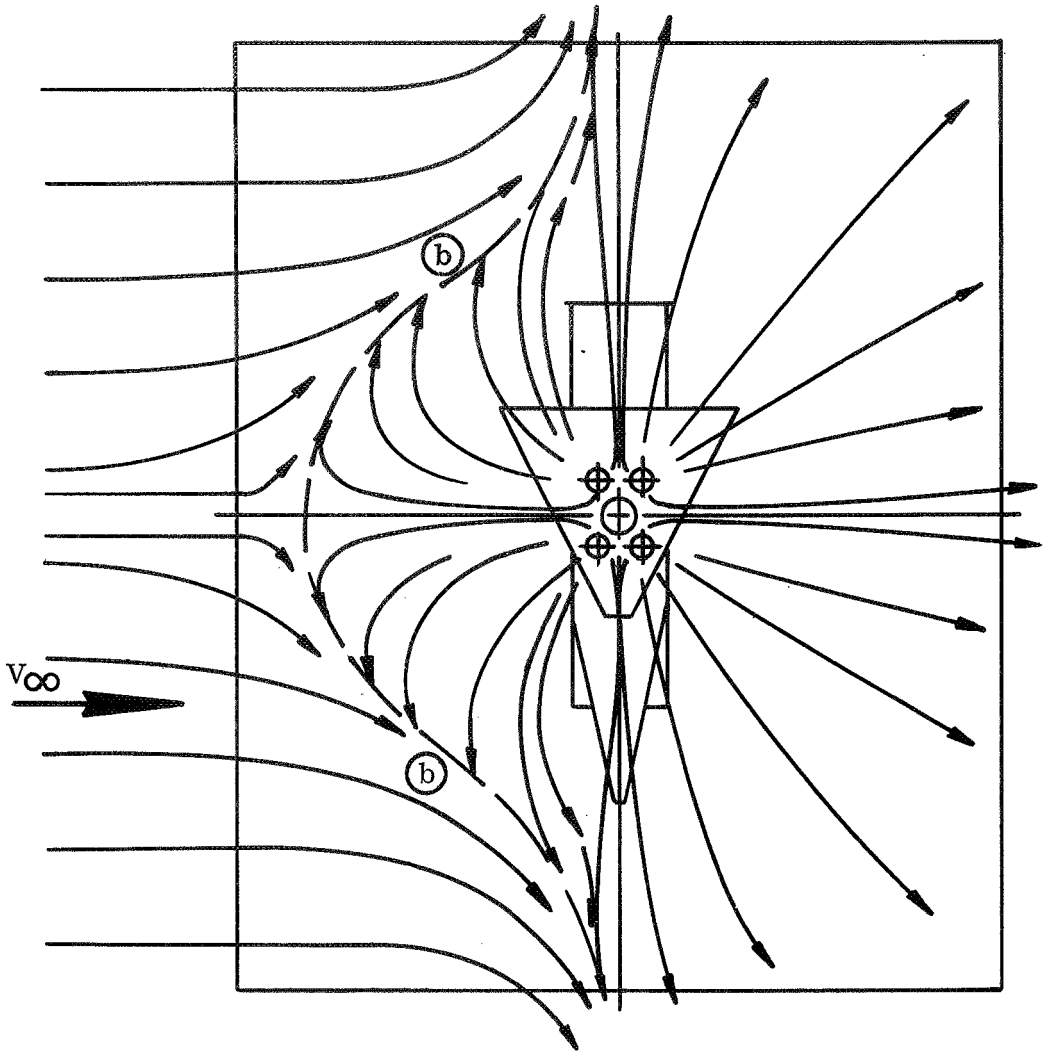


ⓐ Upwash or Fountain
ⓑ Ground Jet Separation Line
ⓒ Eddy at Separation Line
ⓓ Eddy Trapped Under Wing

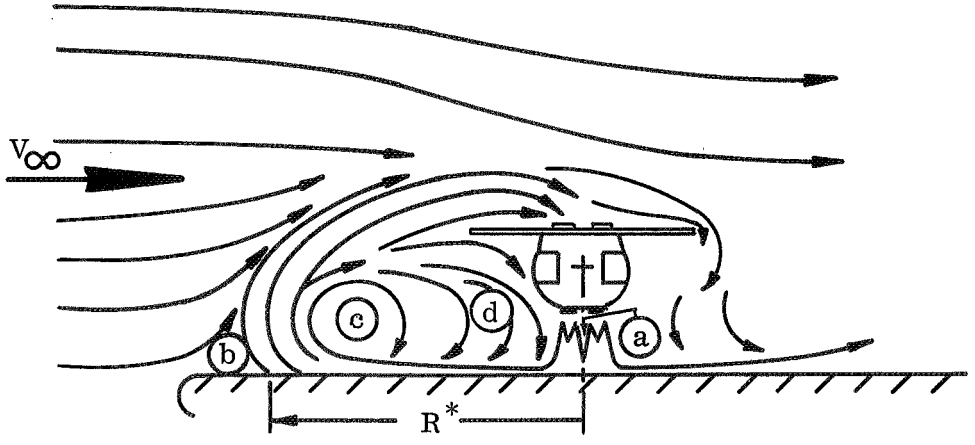


Figure 2. - Effect Of Wind On Recirculation

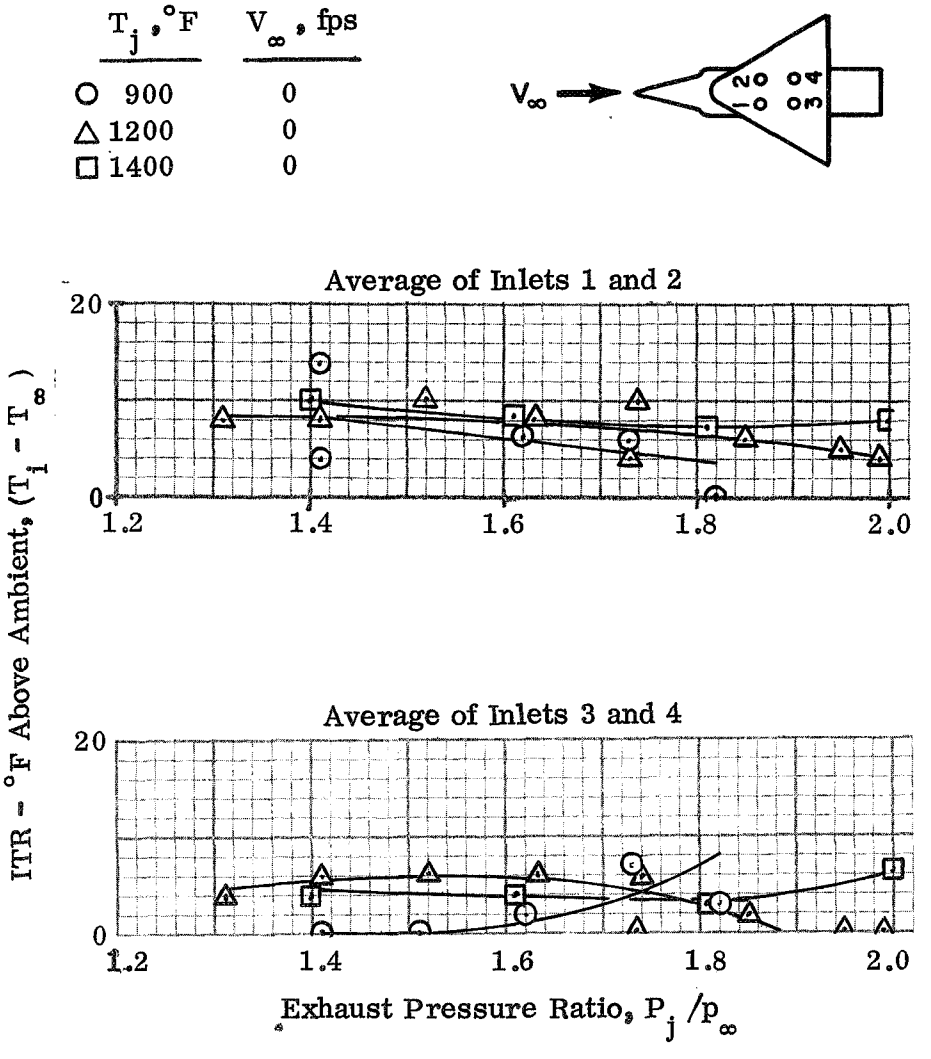


Figure 3. - Variation of ITR With Exhaust Pressure Ratio and Exhaust Temperature at Various Wind Velocities. Top Inlets Configuration, $\psi = 0°$.

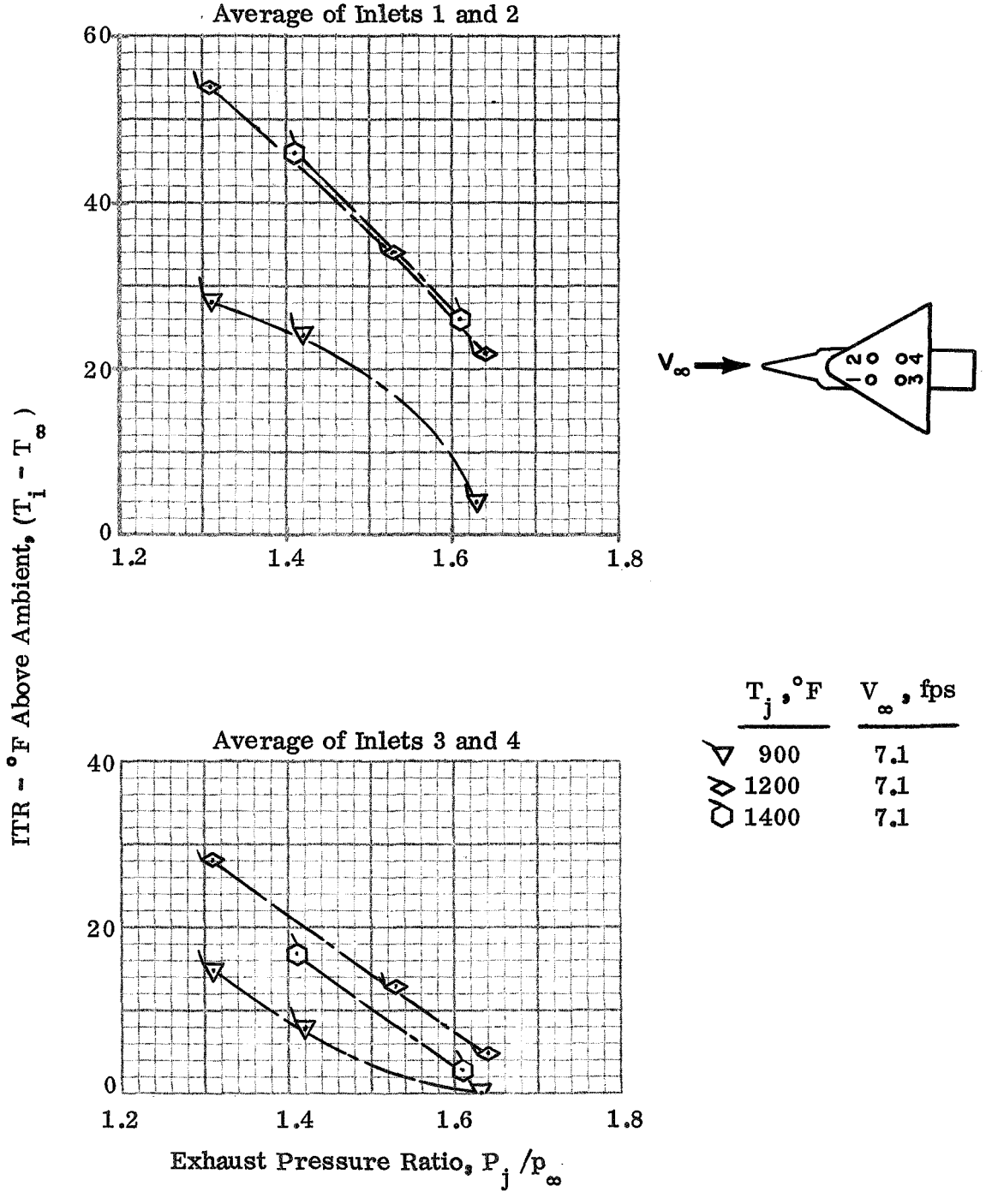


Figure 3. - Continued.

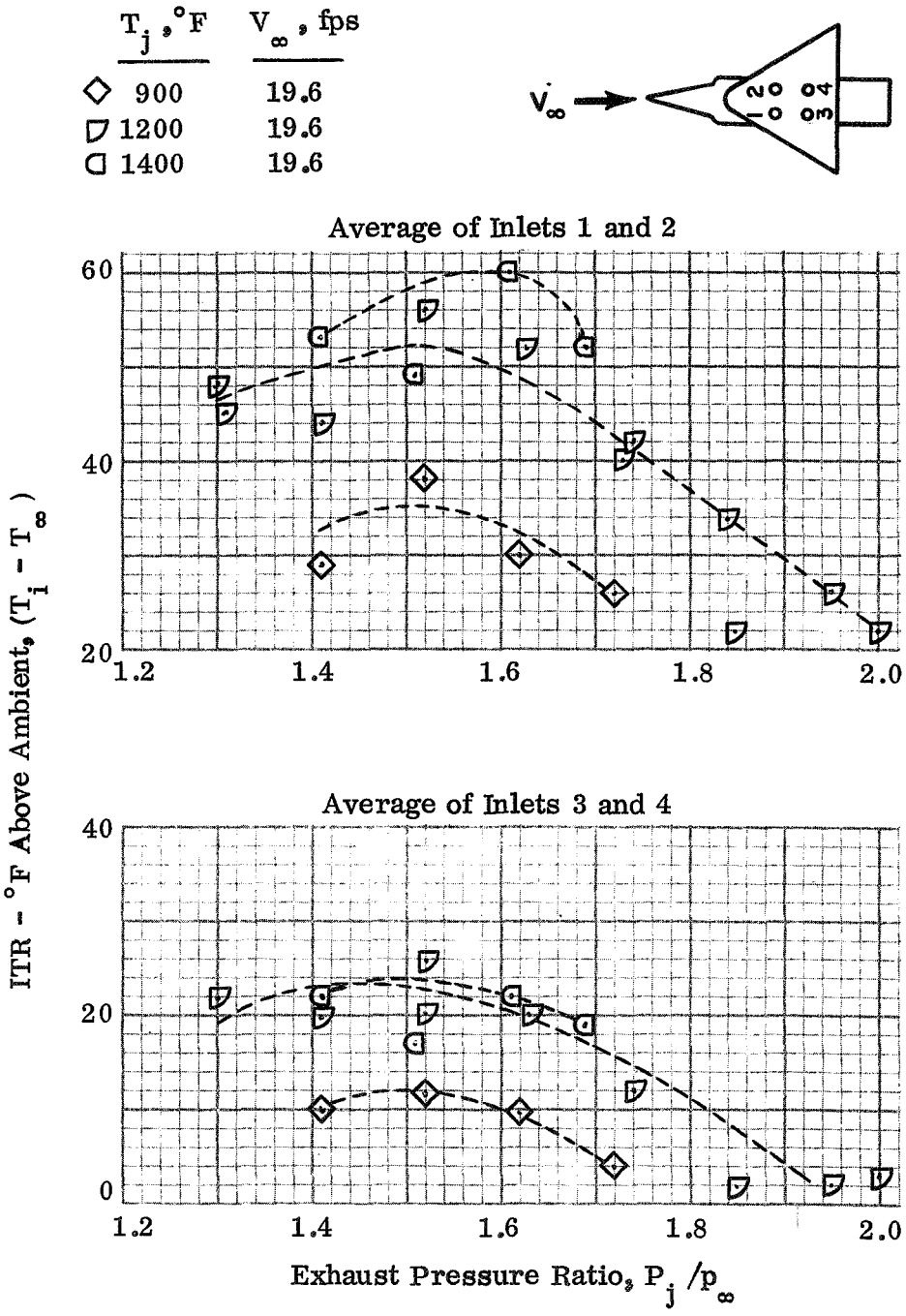


Figure 3. - Continued.

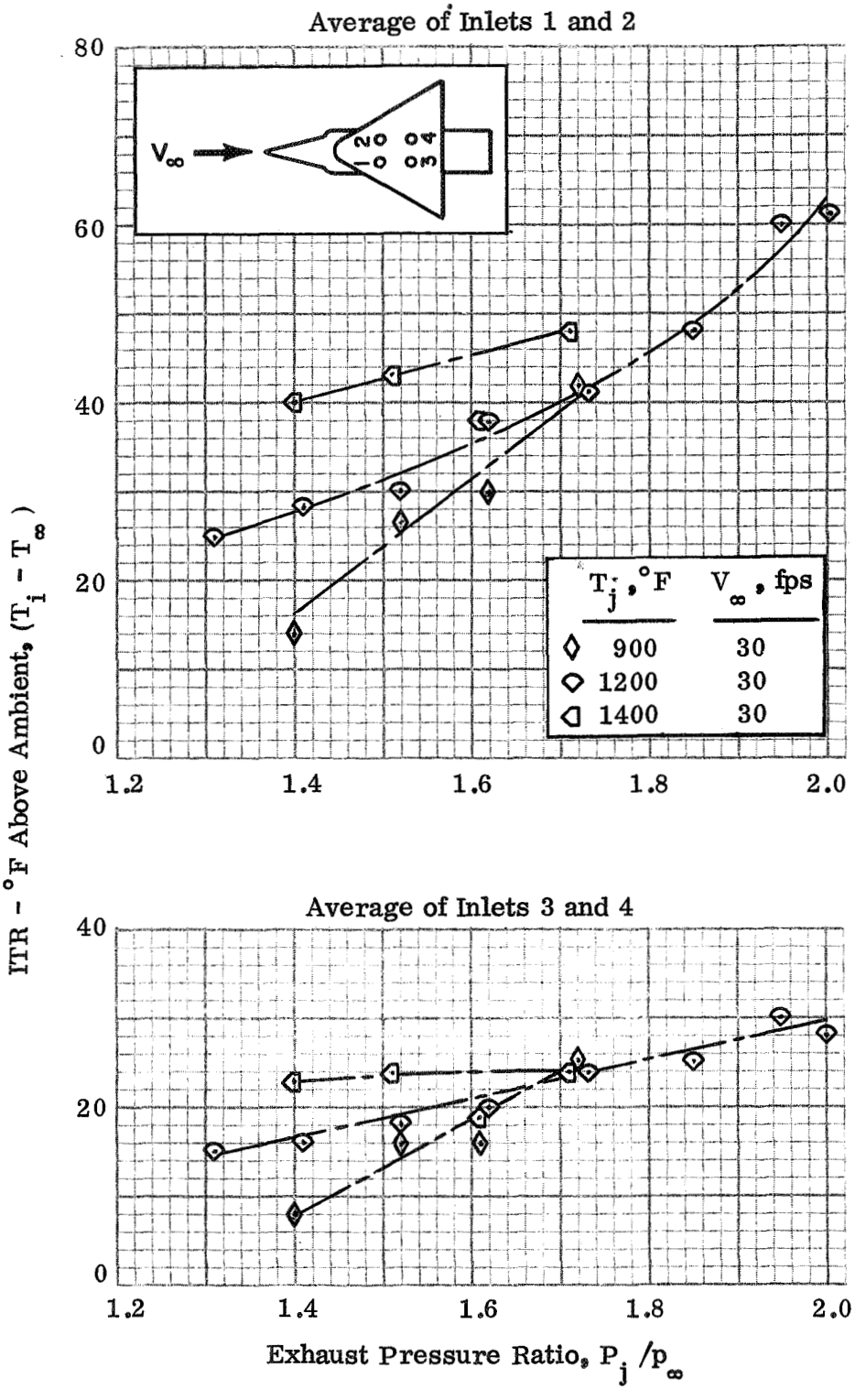


Figure 3. - Continued.

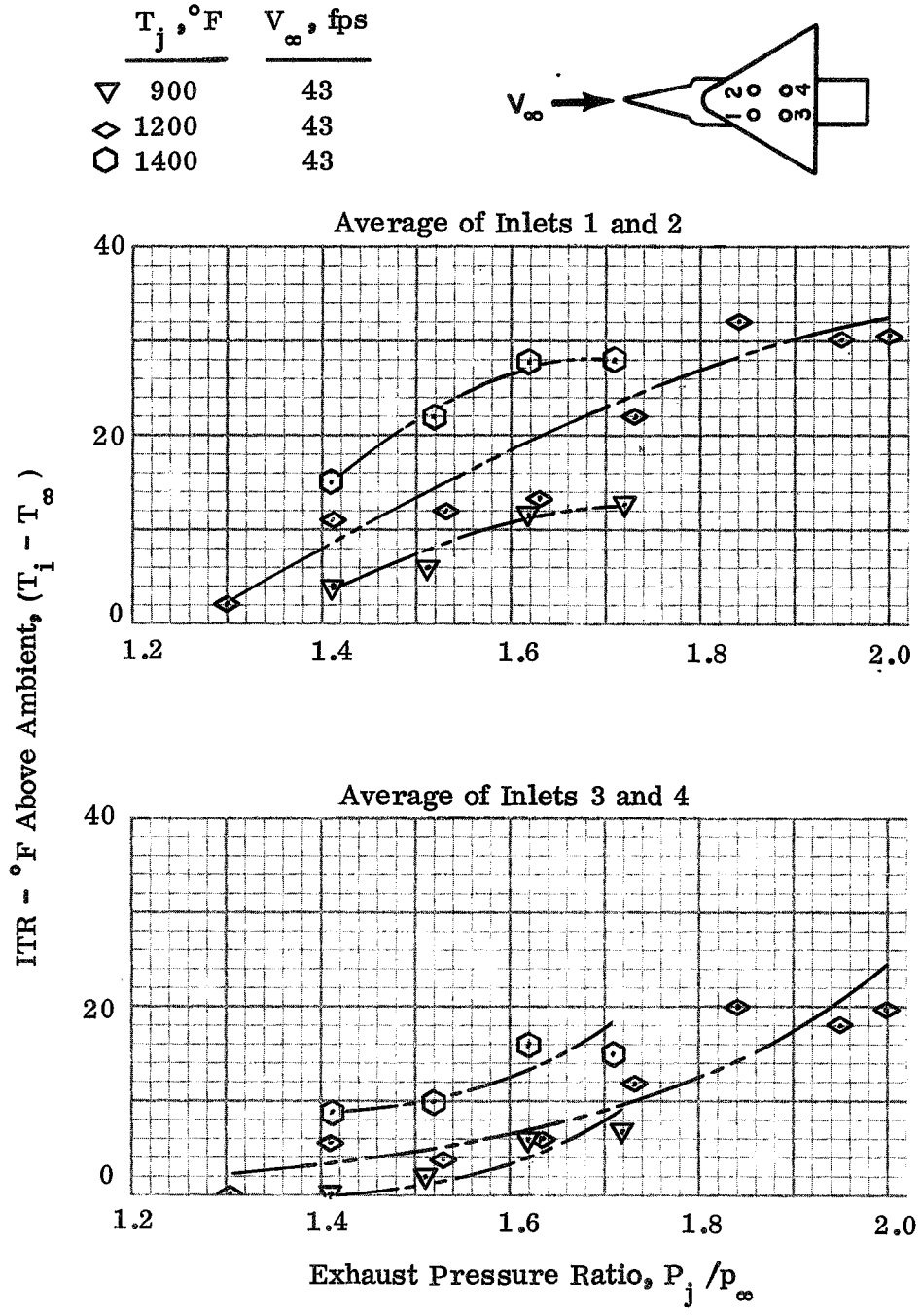


Figure 3. - Continued.

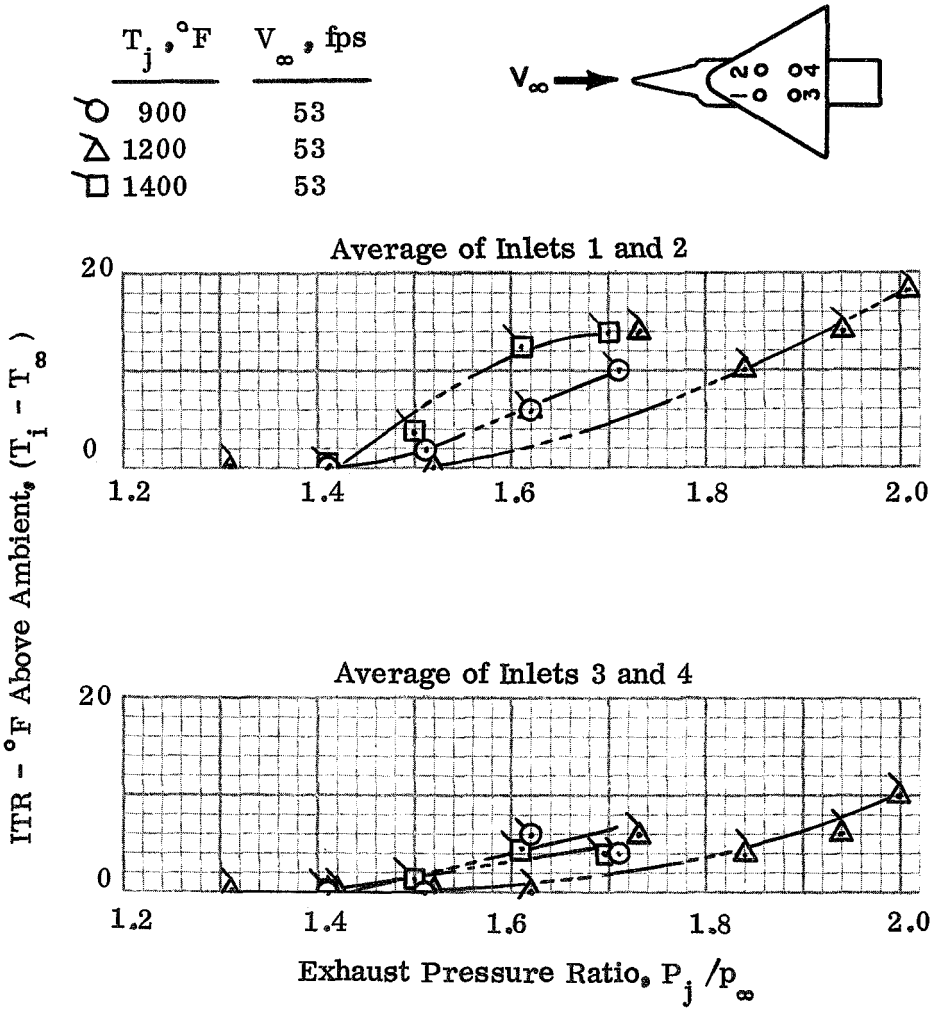


Figure 3. - Concluded.

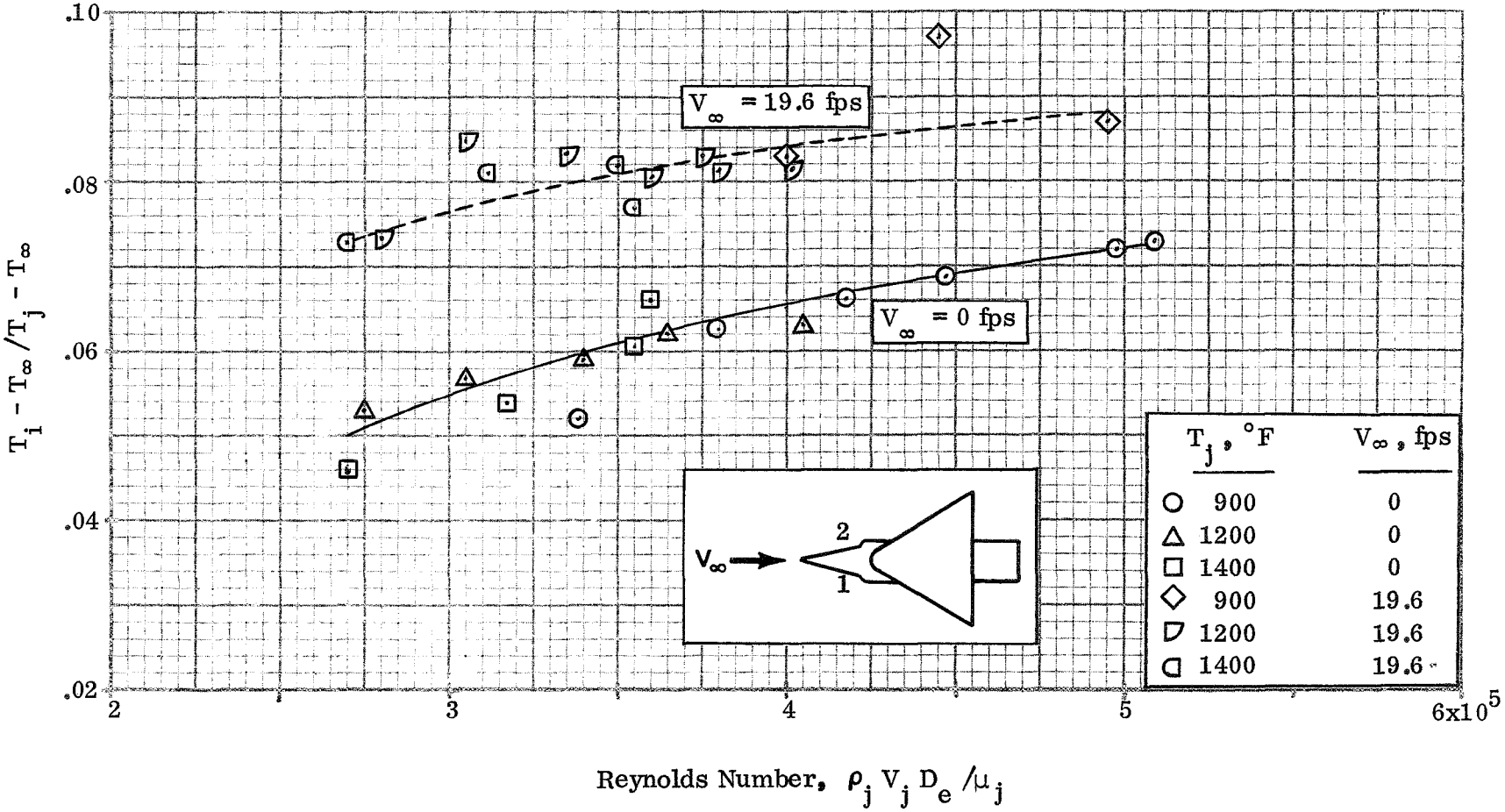


Figure 4. - Correlation of Normalized ITR With Reynolds Number. Side Inlets Configuration, $\psi = 0°$.

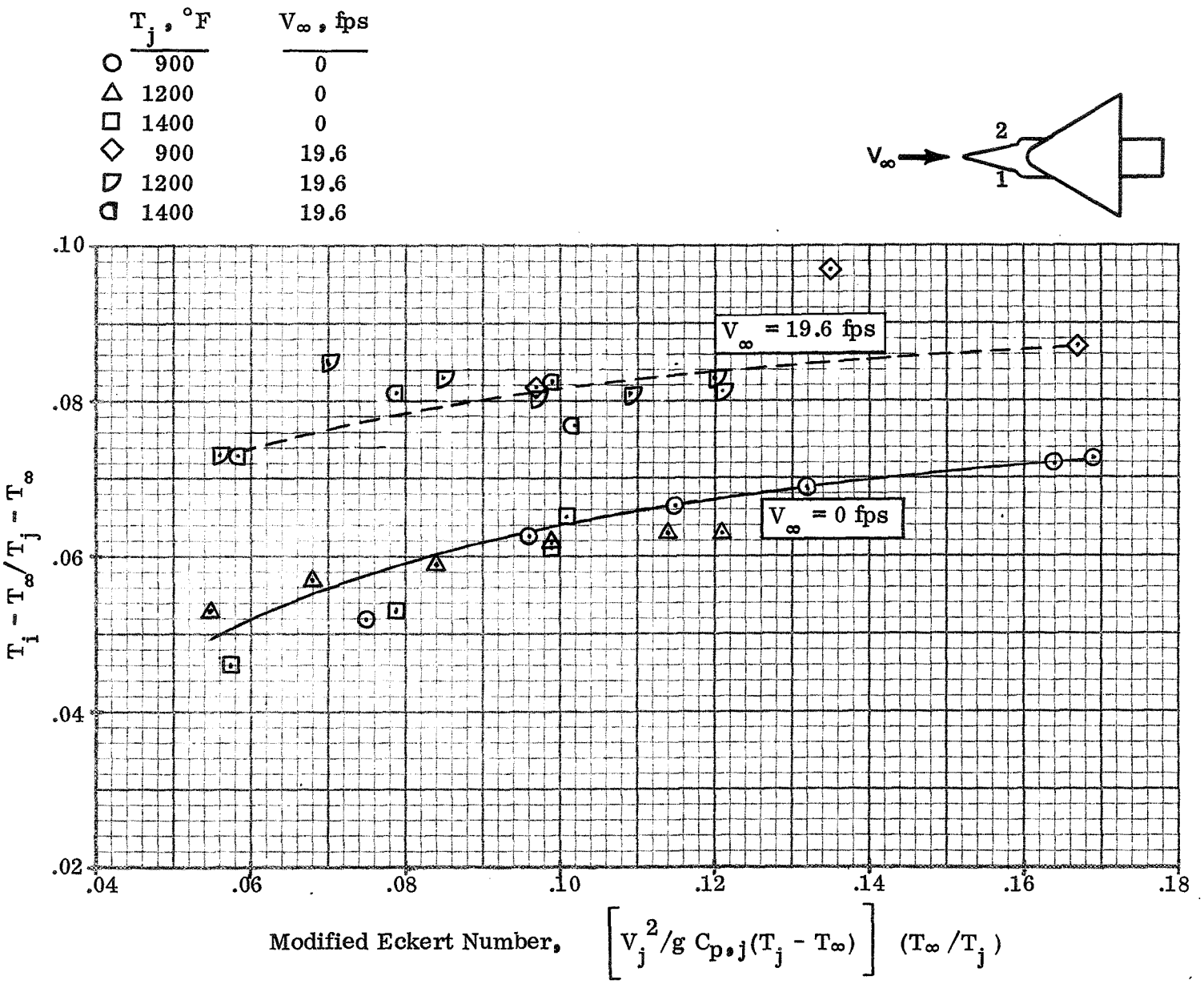


Figure 5. - Correlation of Normalized ITR With Modified Eckert Number. Side Inlets Configuration, $\psi = 0°$.

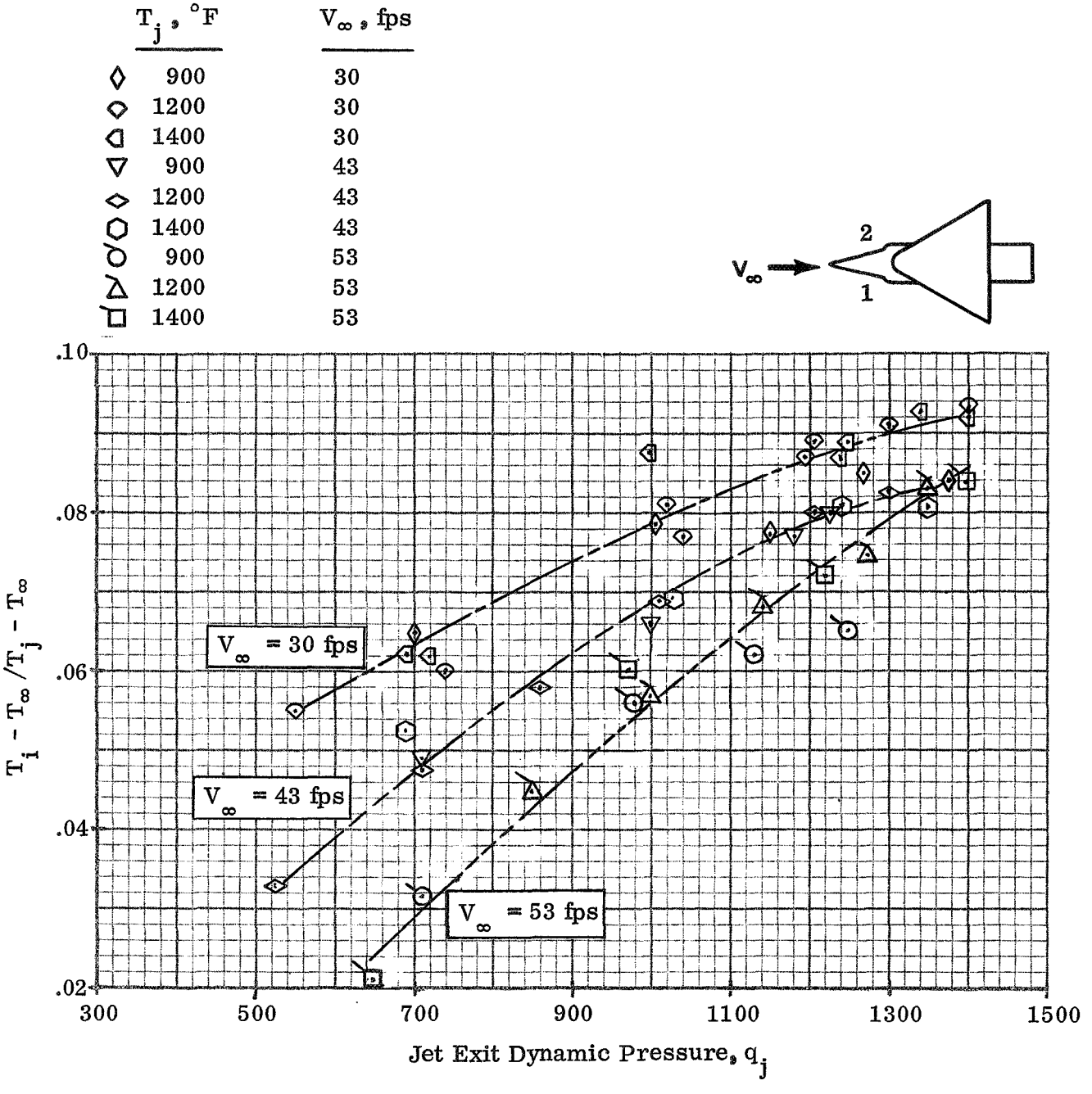


Figure 6. - Correlation of Normalized ITR With Jet Exit Dynamic Pressure. Side Inlets Configuration, $\psi = 0°$.

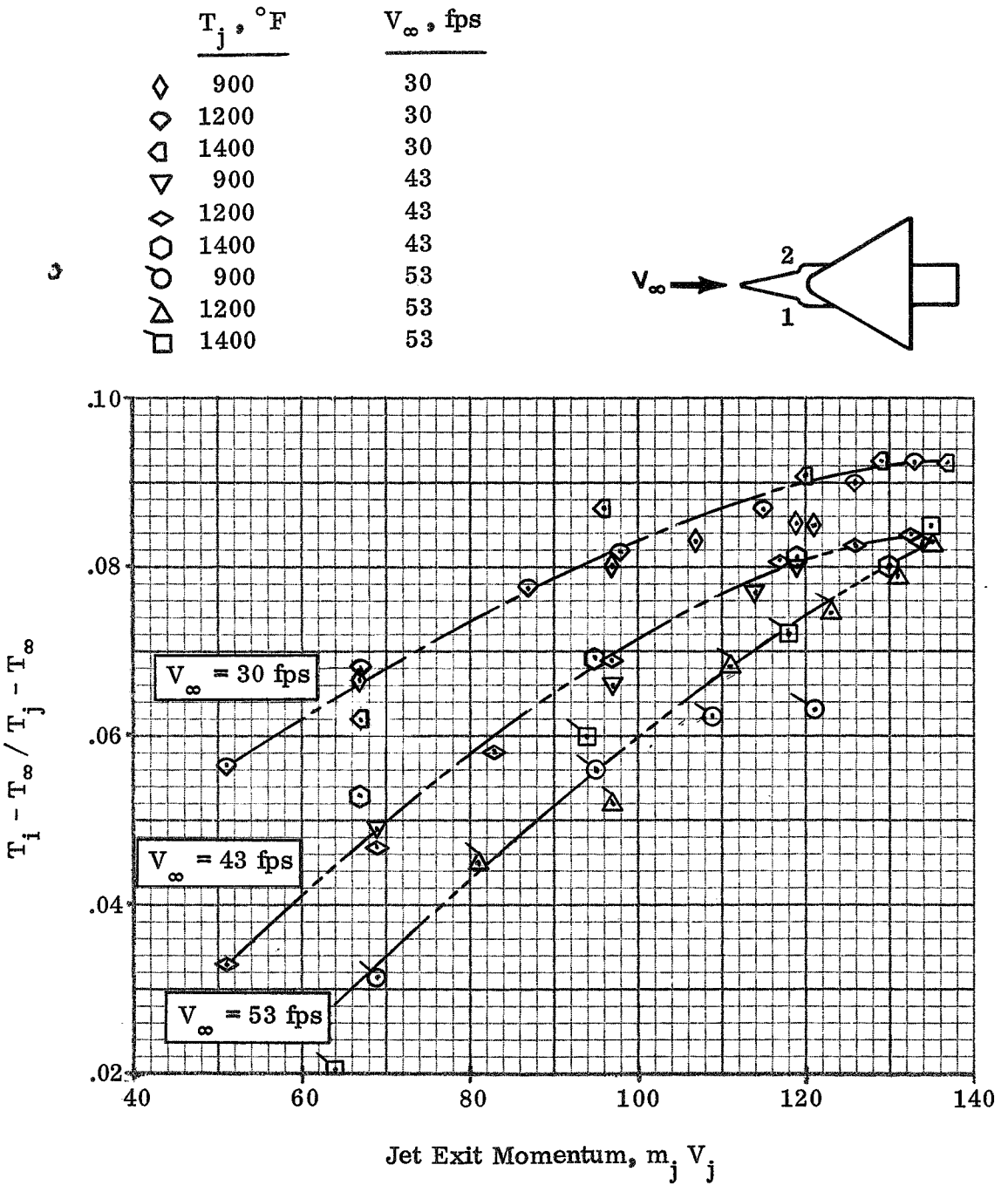


Figure 7. - Correlation of Normalized ITR With Jet Exit Momentum. Side Inlets Configuration, $\psi = 0°$.

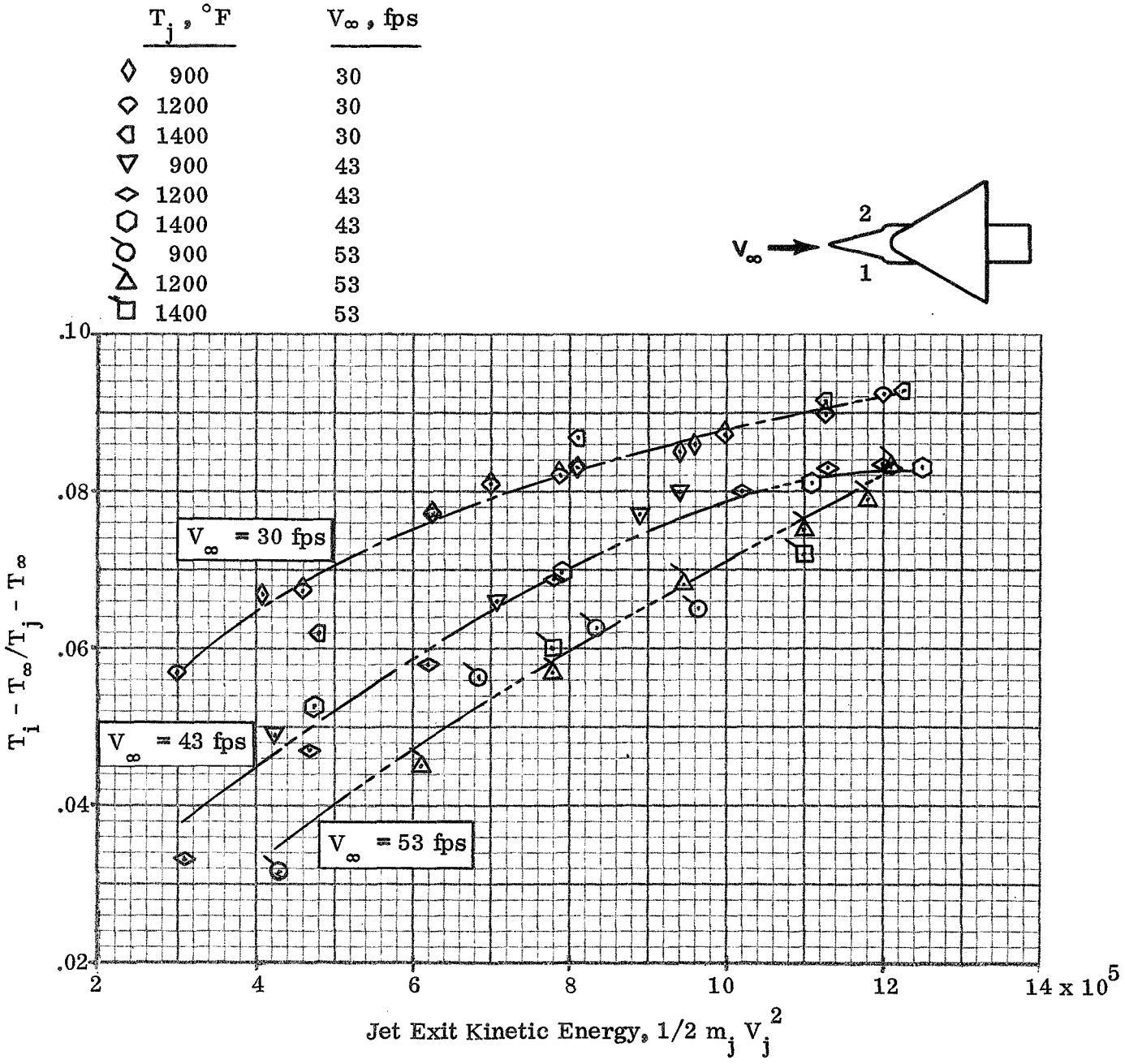


Figure 8. - Correlation of Normalized ITR With Jet Exit Kinetic Energy. Side Inlets Configuration, $\psi = 0°$.

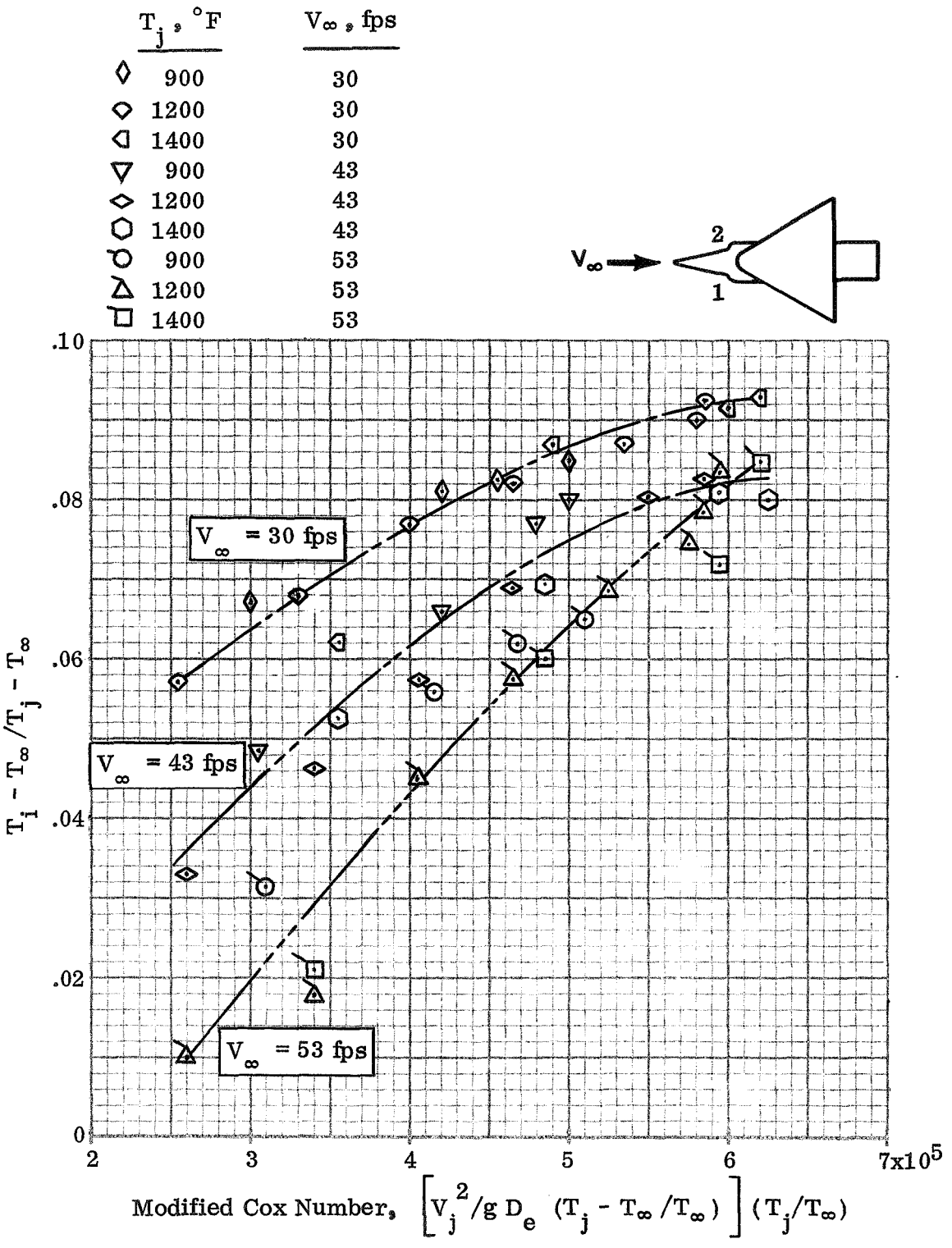


Figure 9. - Correlation of Normalized ITR With Modified Cox Number. Side Inlets Configuration, $\psi = 0°$.

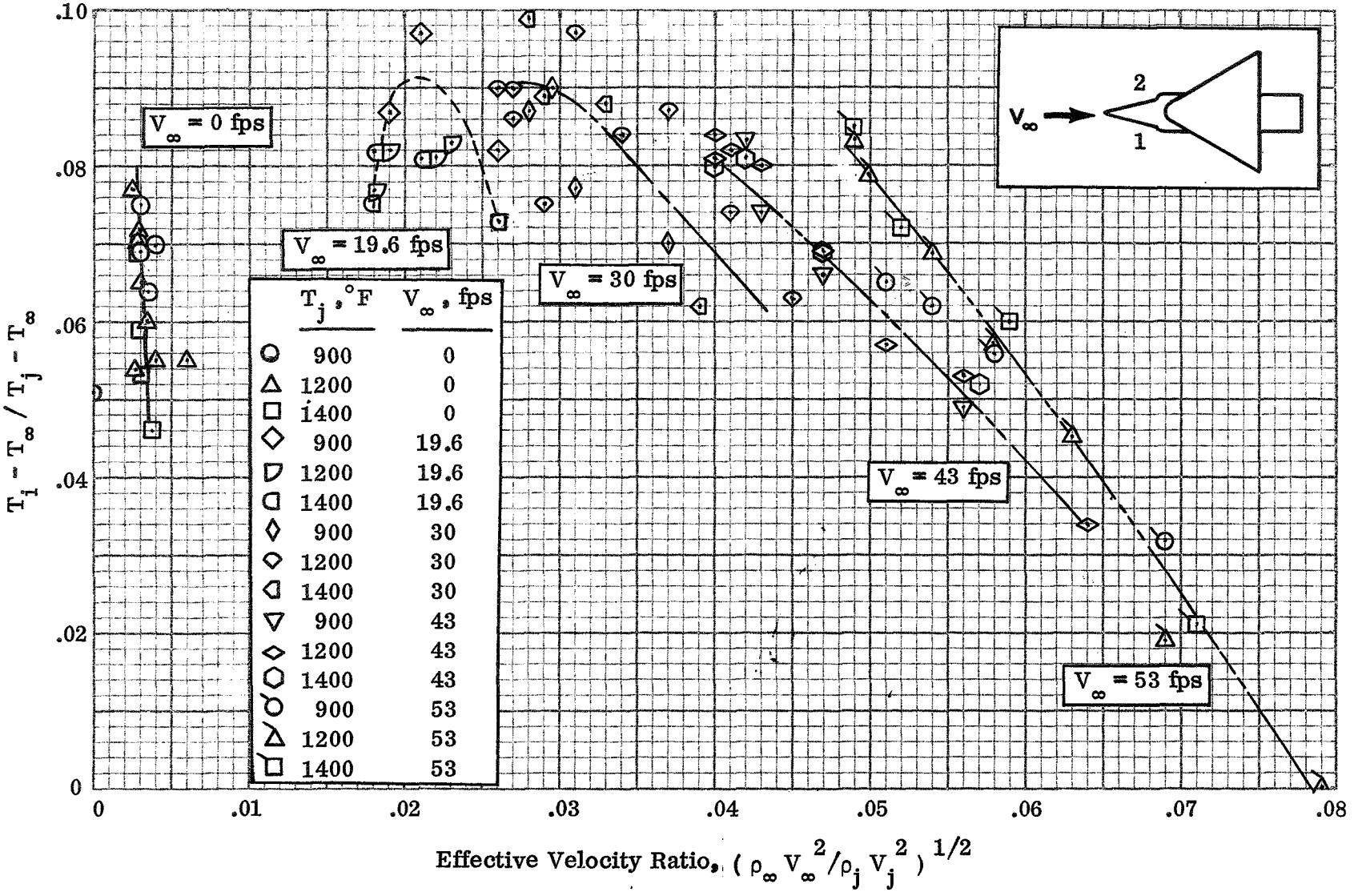


Figure 10. - Variation of Normalized ITR With Effective Velocity Ratio. Side Inlets Configuration, $\psi = 0°$.

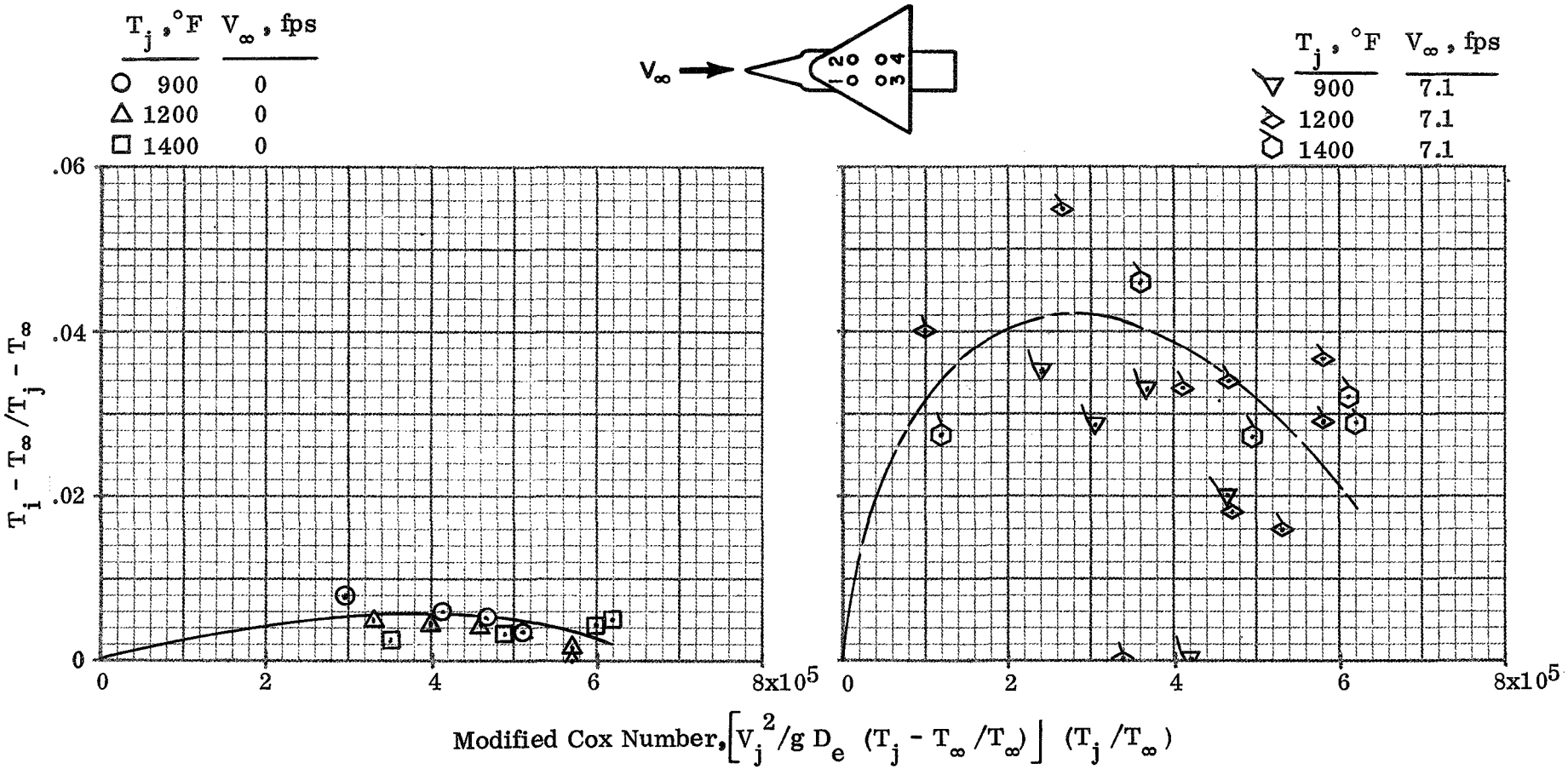


Figure 11. - Correlation of Normalized ITR With Modified Cox Number. Top Inlets Configuration, $\psi = 0°$ (ITR is average of Inlets 1 and 2).

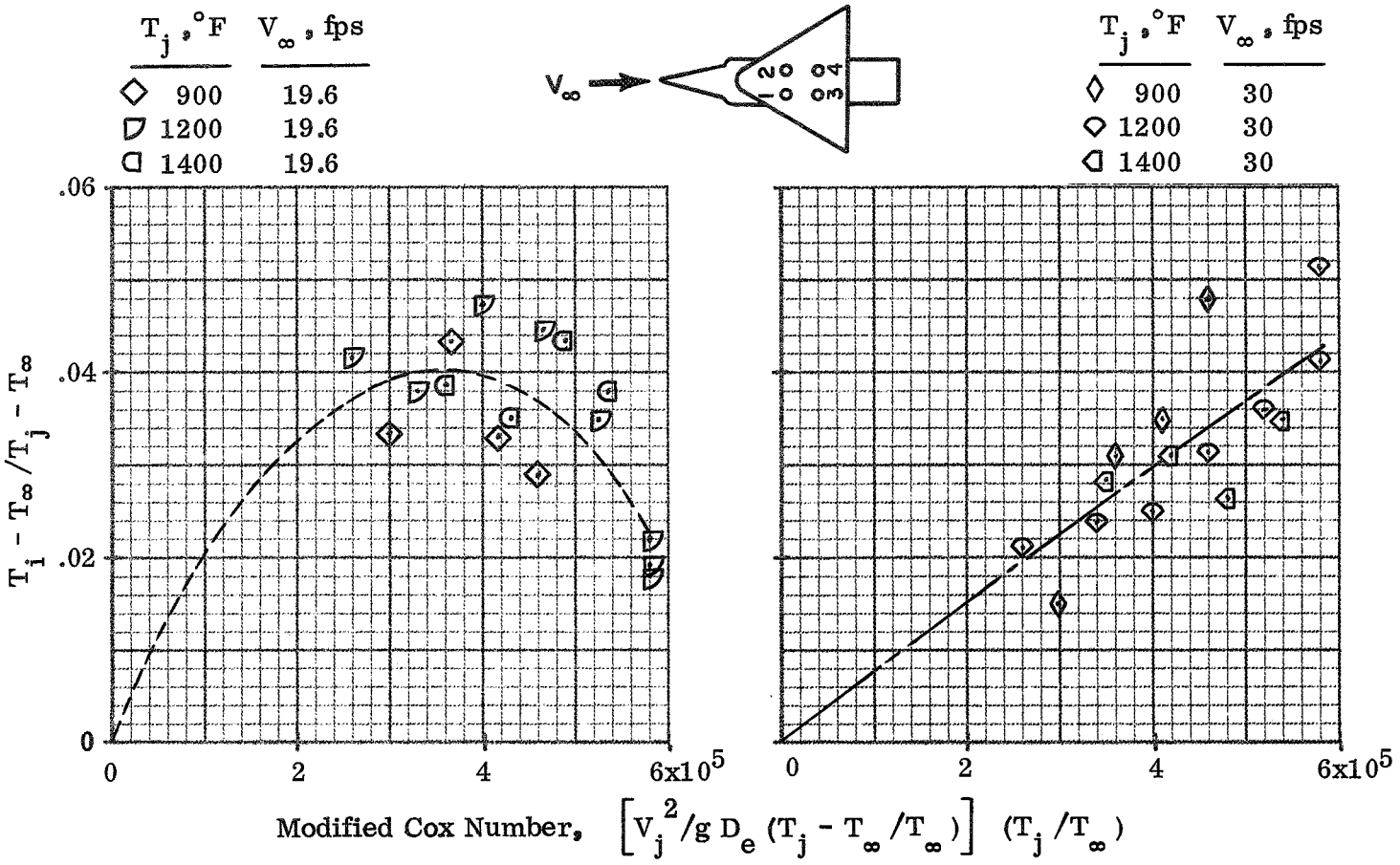


Figure 11. - Continued.

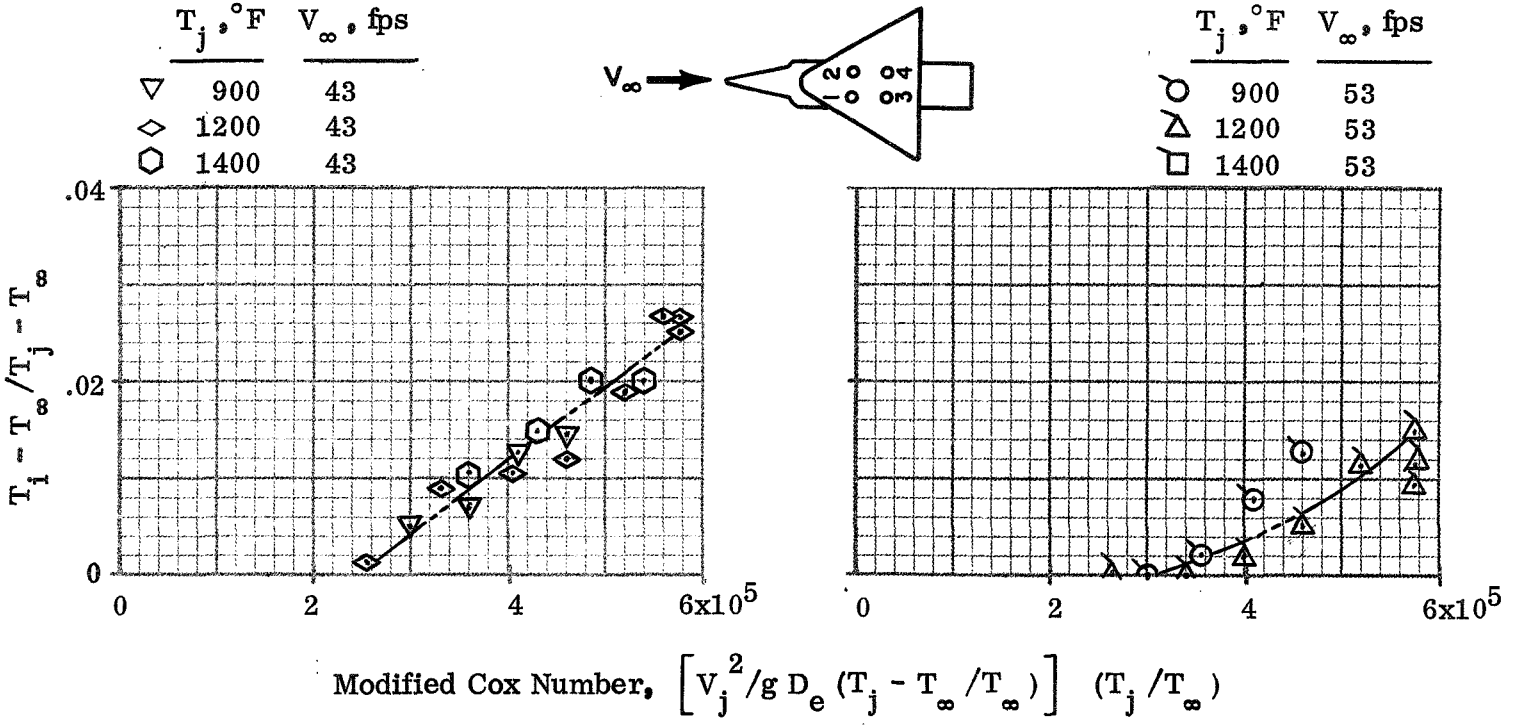


Figure 11. - Concluded.

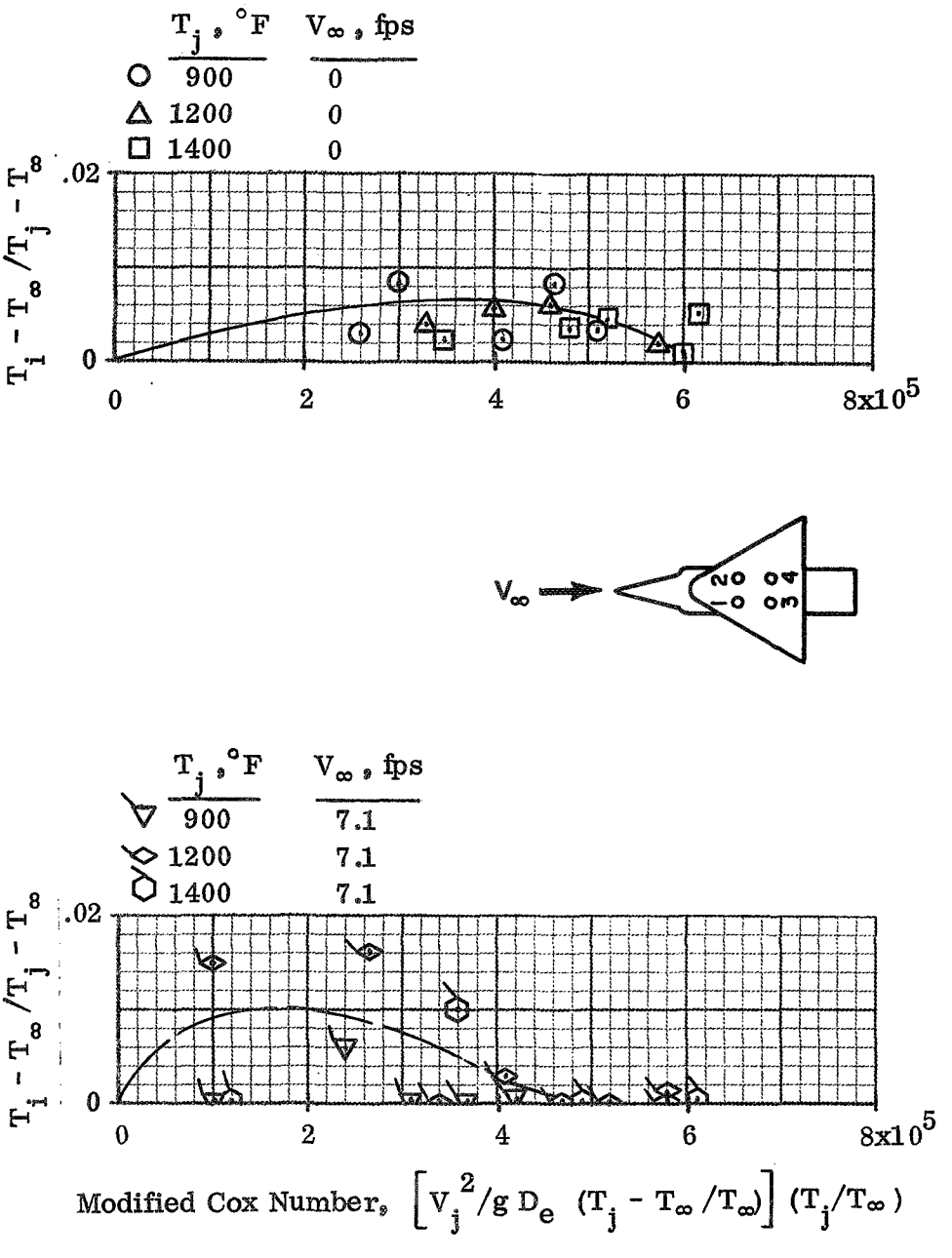


Figure 12. - Correlation of Normalized ITR With Modified Cox Number. Top Inlets Configurations, $\psi = 0°$ (ITR is average of Inlets 3 and 4).

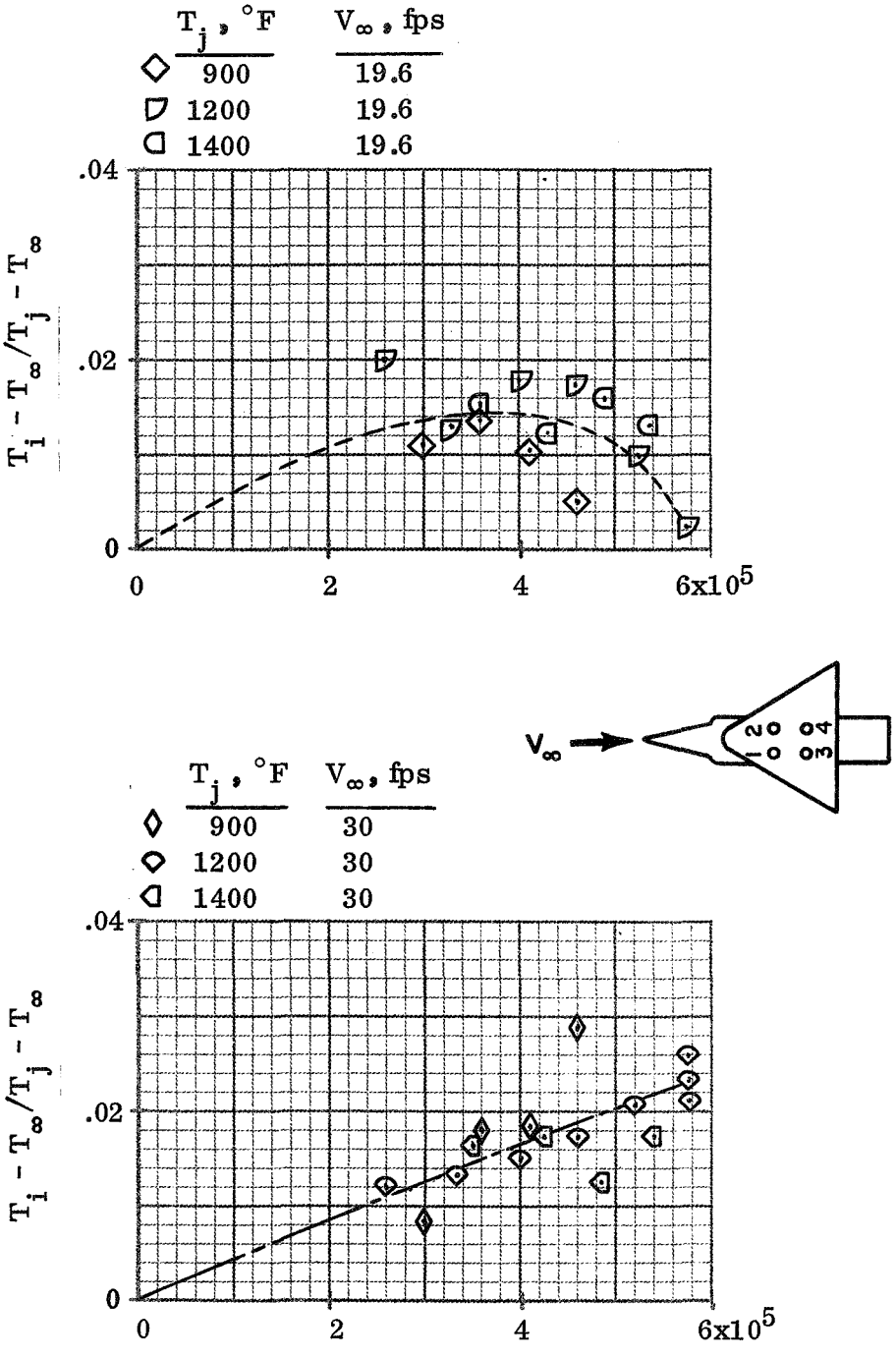


Figure 12. - Continued.

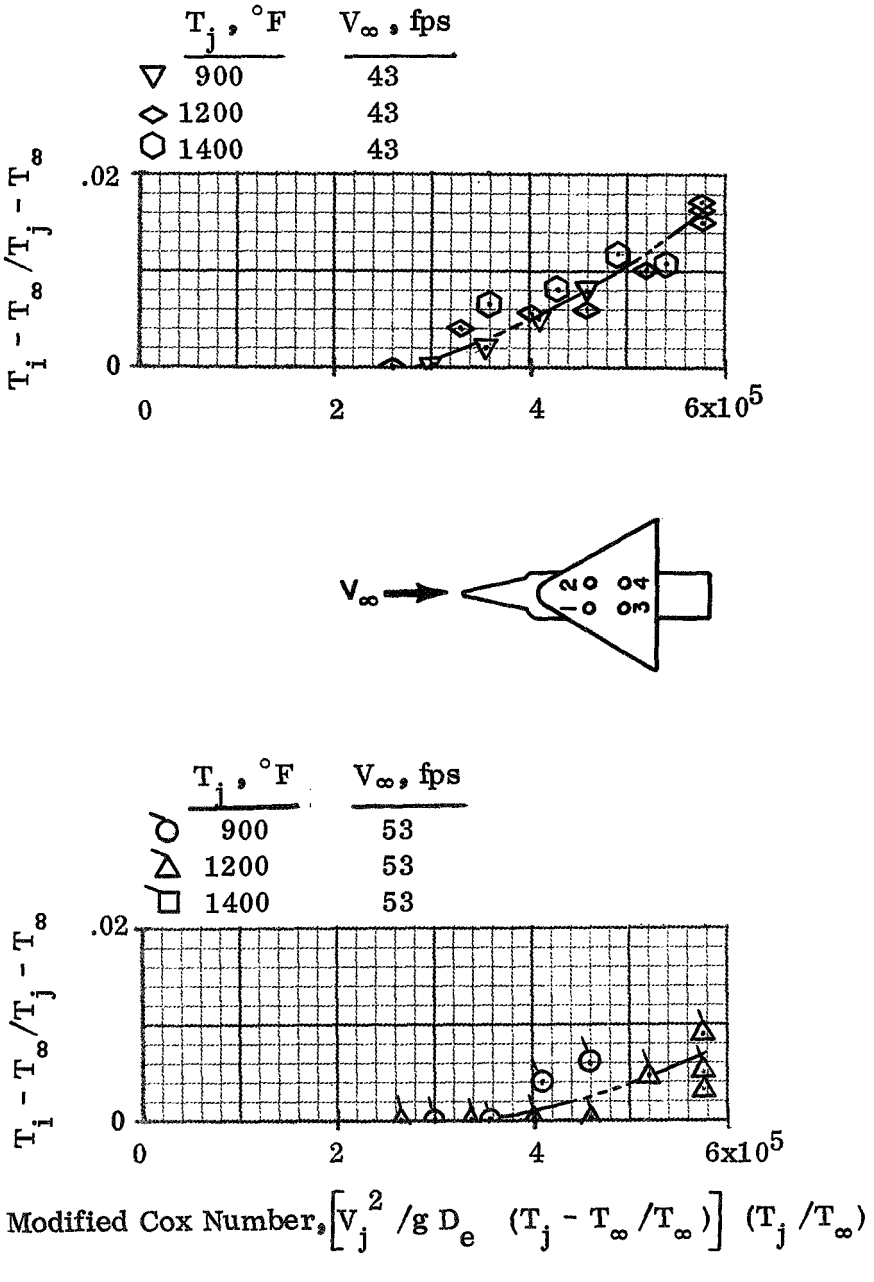


Figure 12. - Concluded.

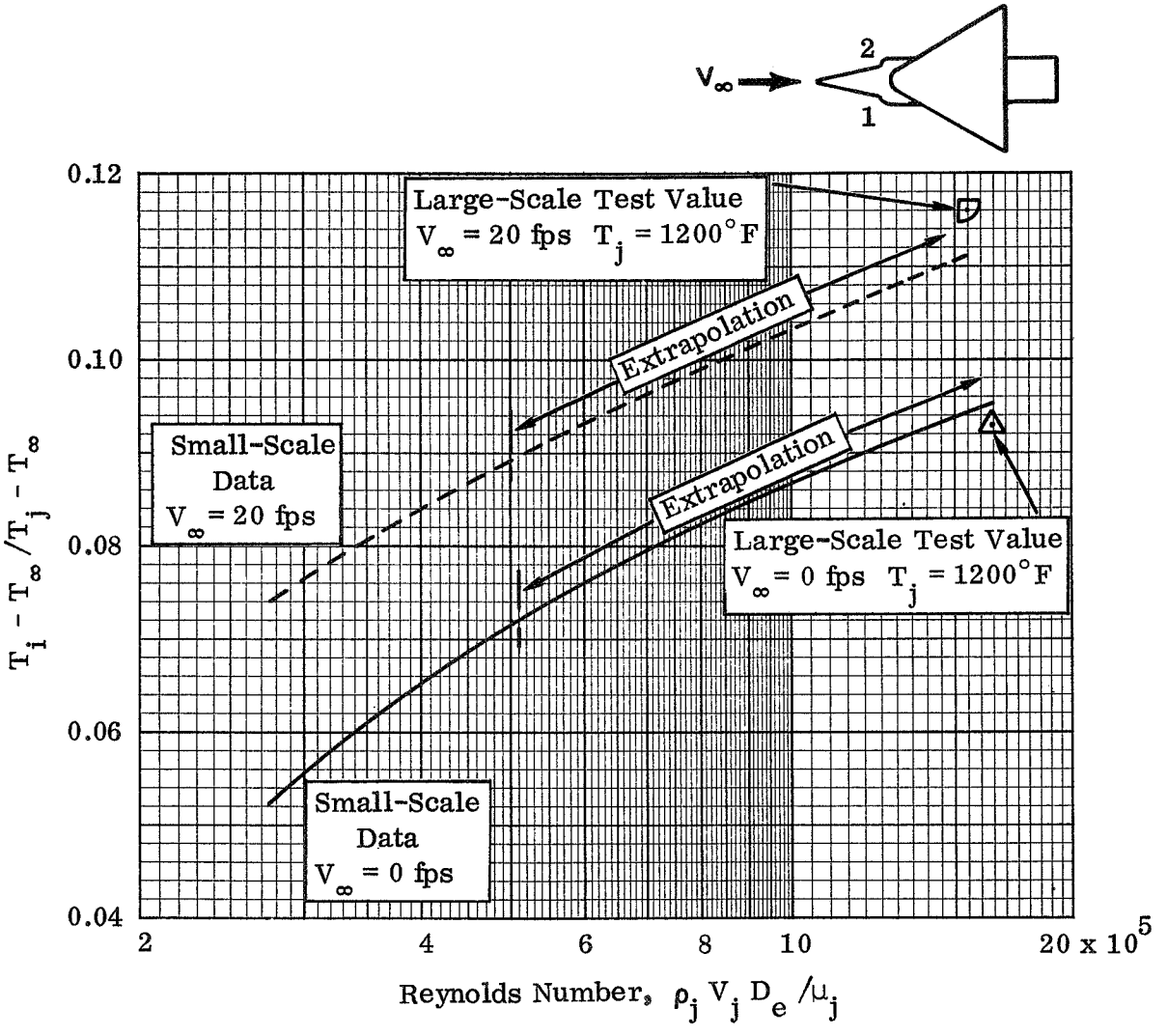


Figure 13. - Comparison of Small and Large-Scale ITR Based On Equal Reynolds Number. Side Inlets Configuration, $\psi = 0°$.

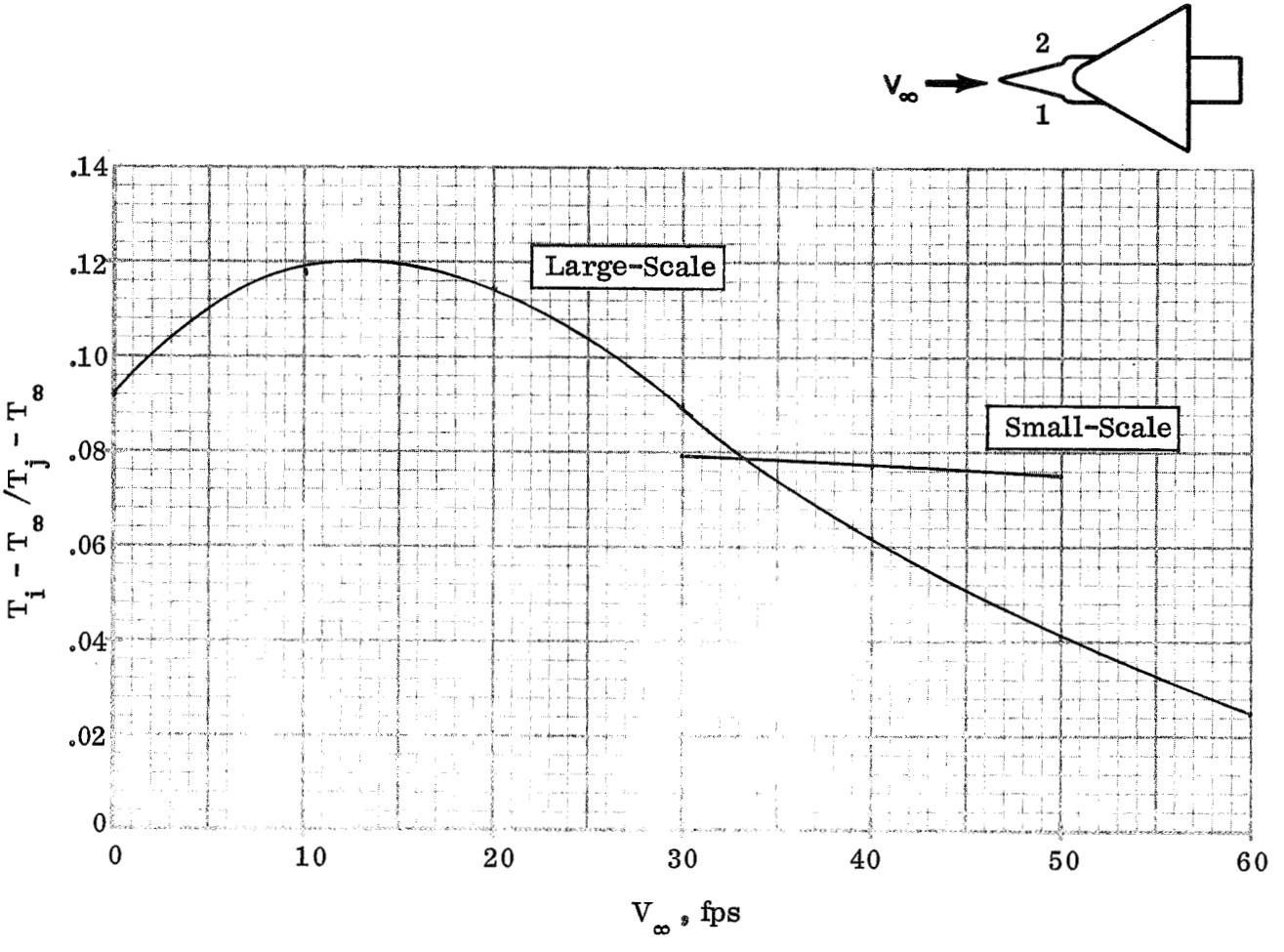


Figure 14. - Comparison of Small and Large-Scale ITR vs $V_\infty$ at Equal $q_j$. Side Inlets Configuration, $\psi = 0°$.

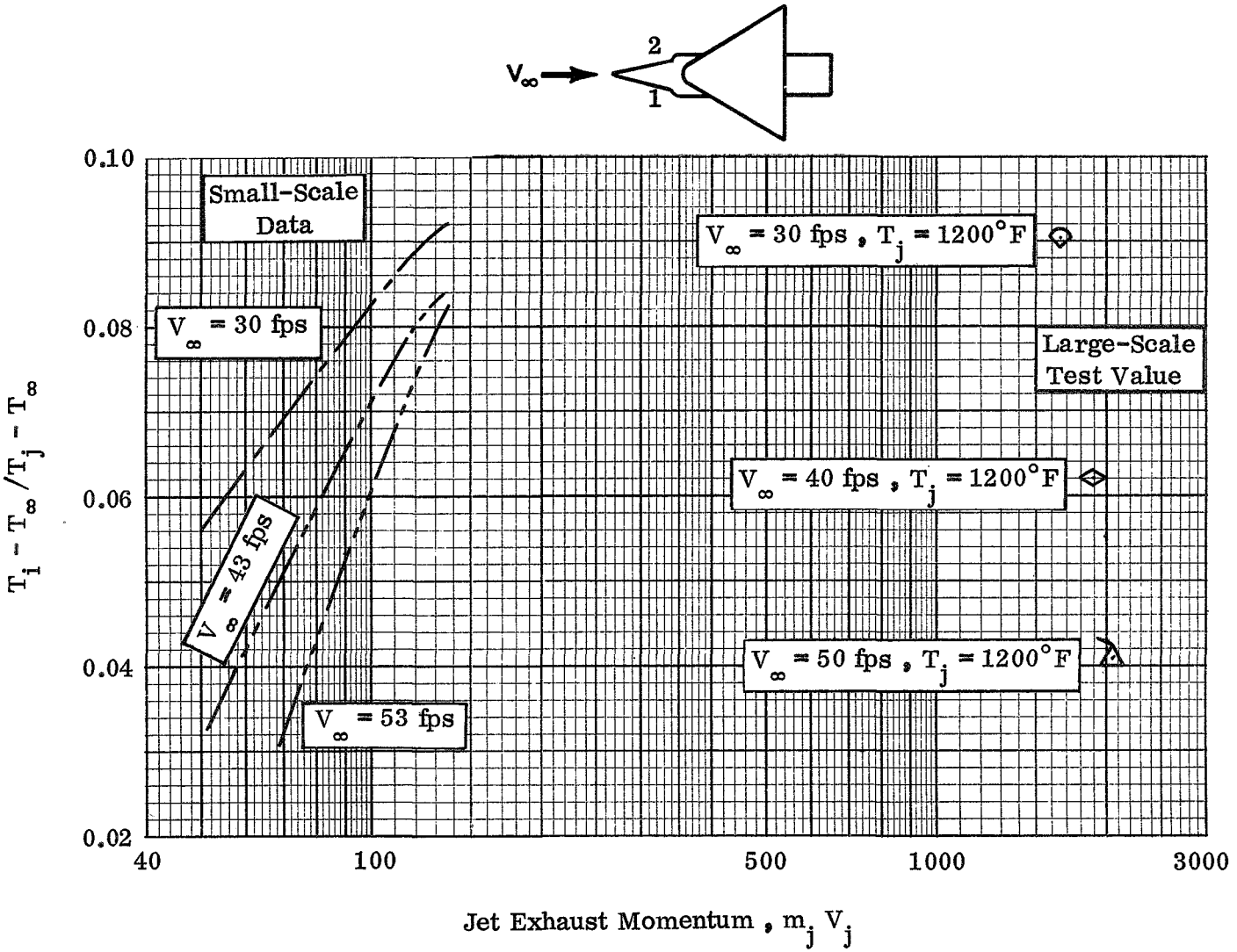


Figure 15. - Comparison of Small and Large-Scale ITR Based on Jet Exhaust Momentum. Side Inlets Configuration, $\psi = 0°$.

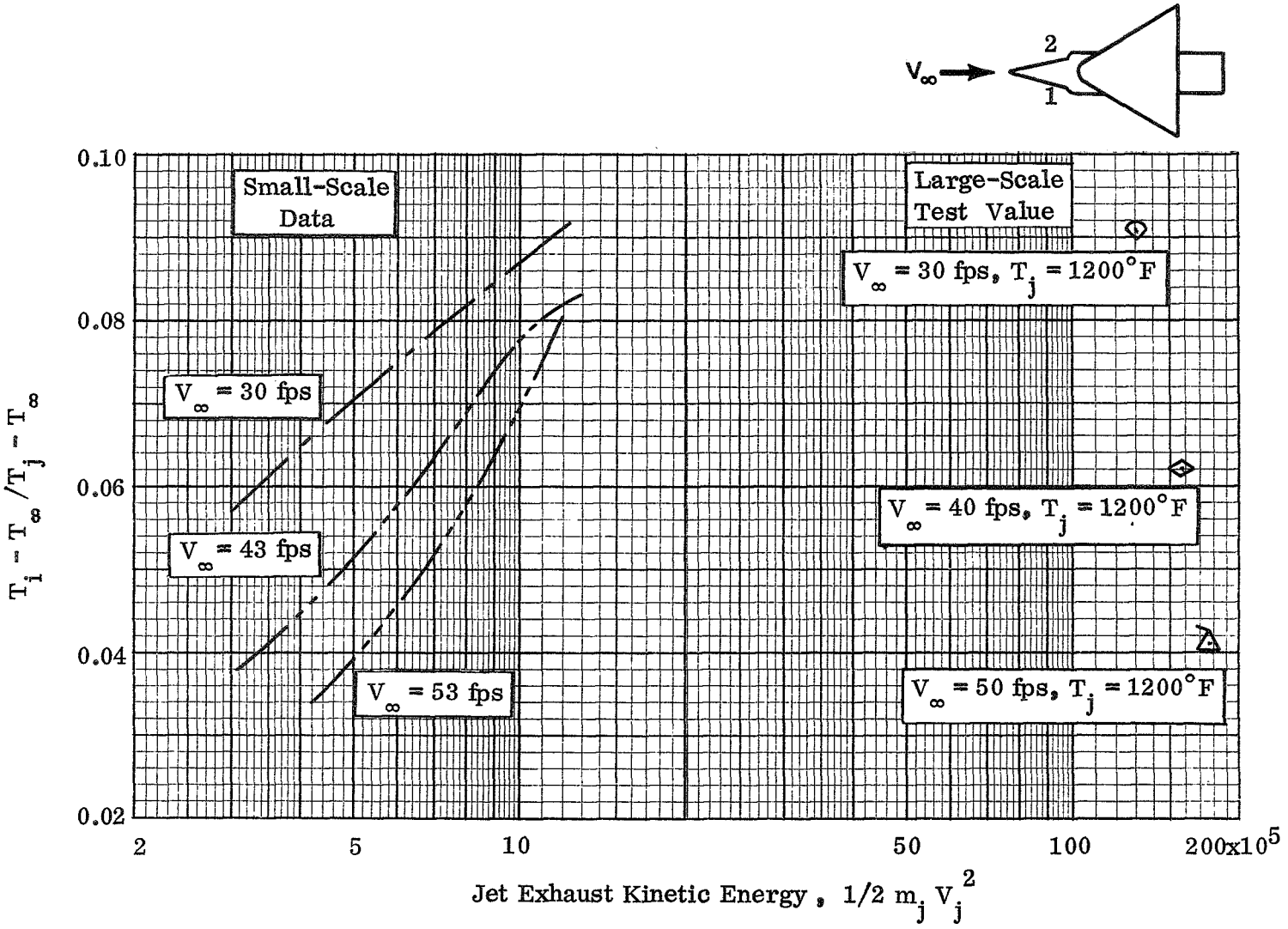


Figure 16. - Comparison of Small and Large-Scale ITR Based on Jet Exhaust Kinetic Energy. Side Inlets Configuration, $\psi = 0°$.

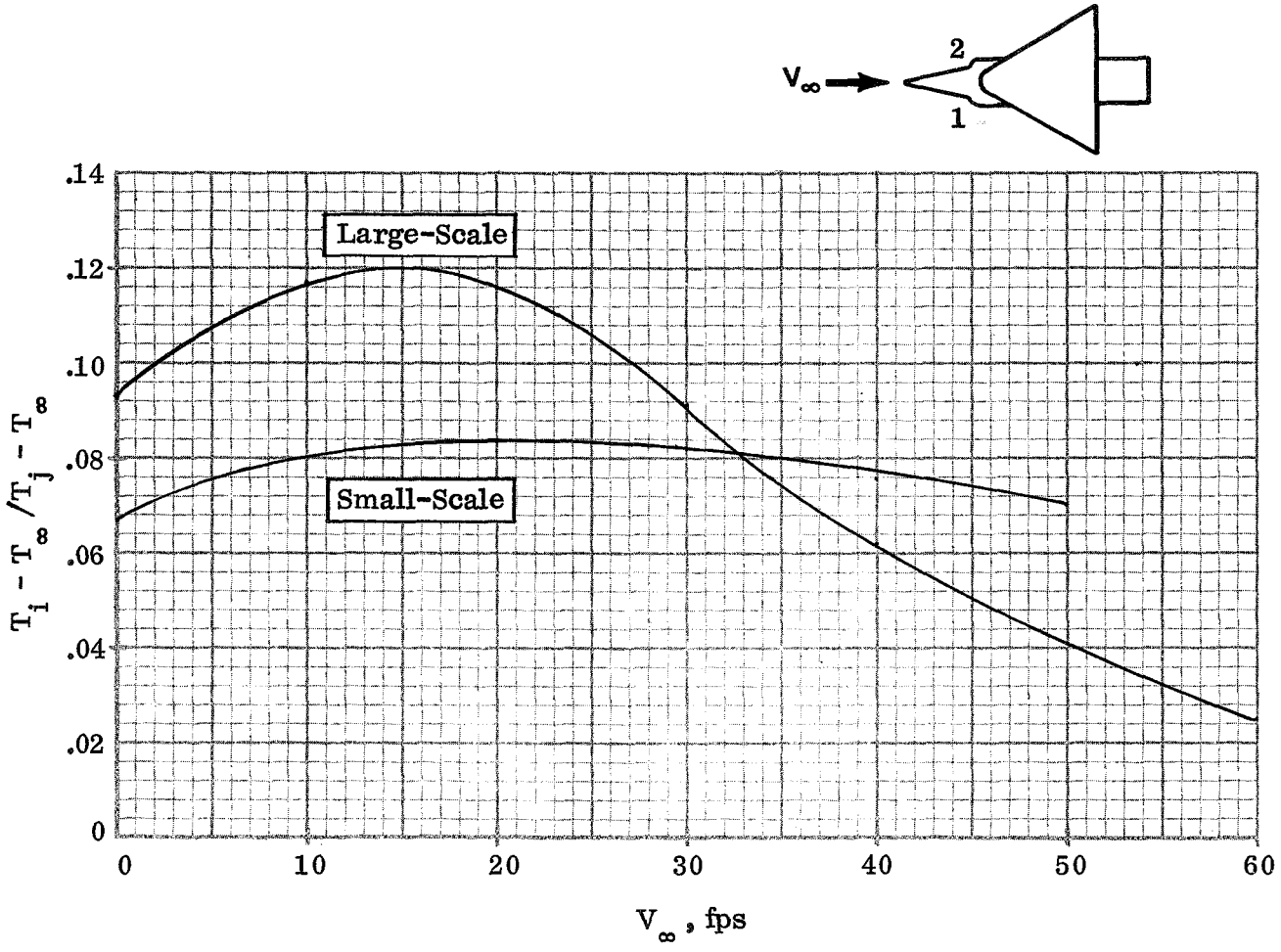


Figure 17. - Comparison of Small and Large-Scale ITR vs $V_\infty$ at Equal $V_j$ and $T_j$. Side Inlets Configuration, $\psi = 0°$

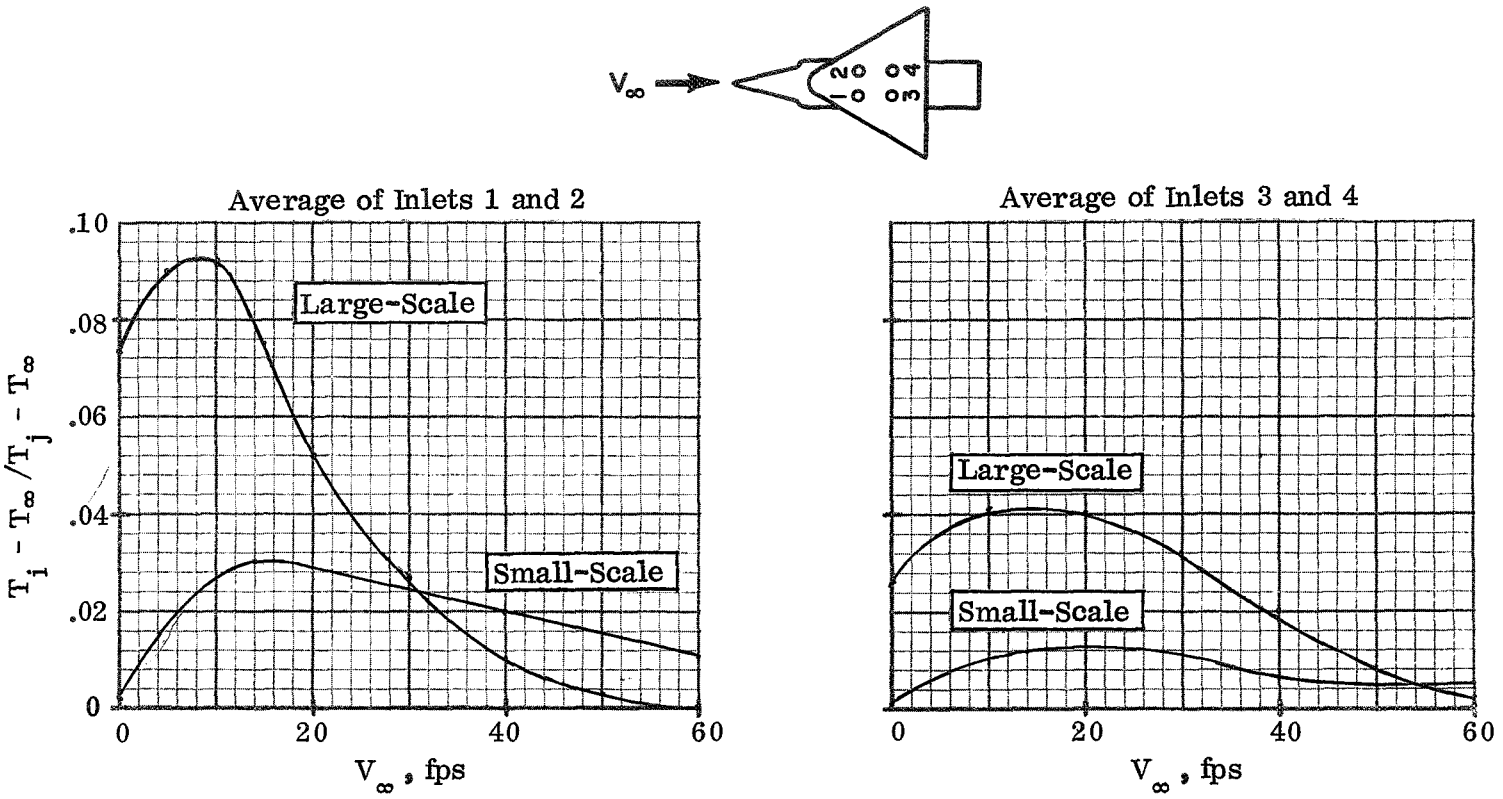


Figure 18. - Comparison of Small and Large-Scale ITR vs $V_\infty$ at Equal Modified Cox Number and Equal $(q_\infty / q_j)^{1/2}$. Top Inlets Configuration, $\psi = 0°$.

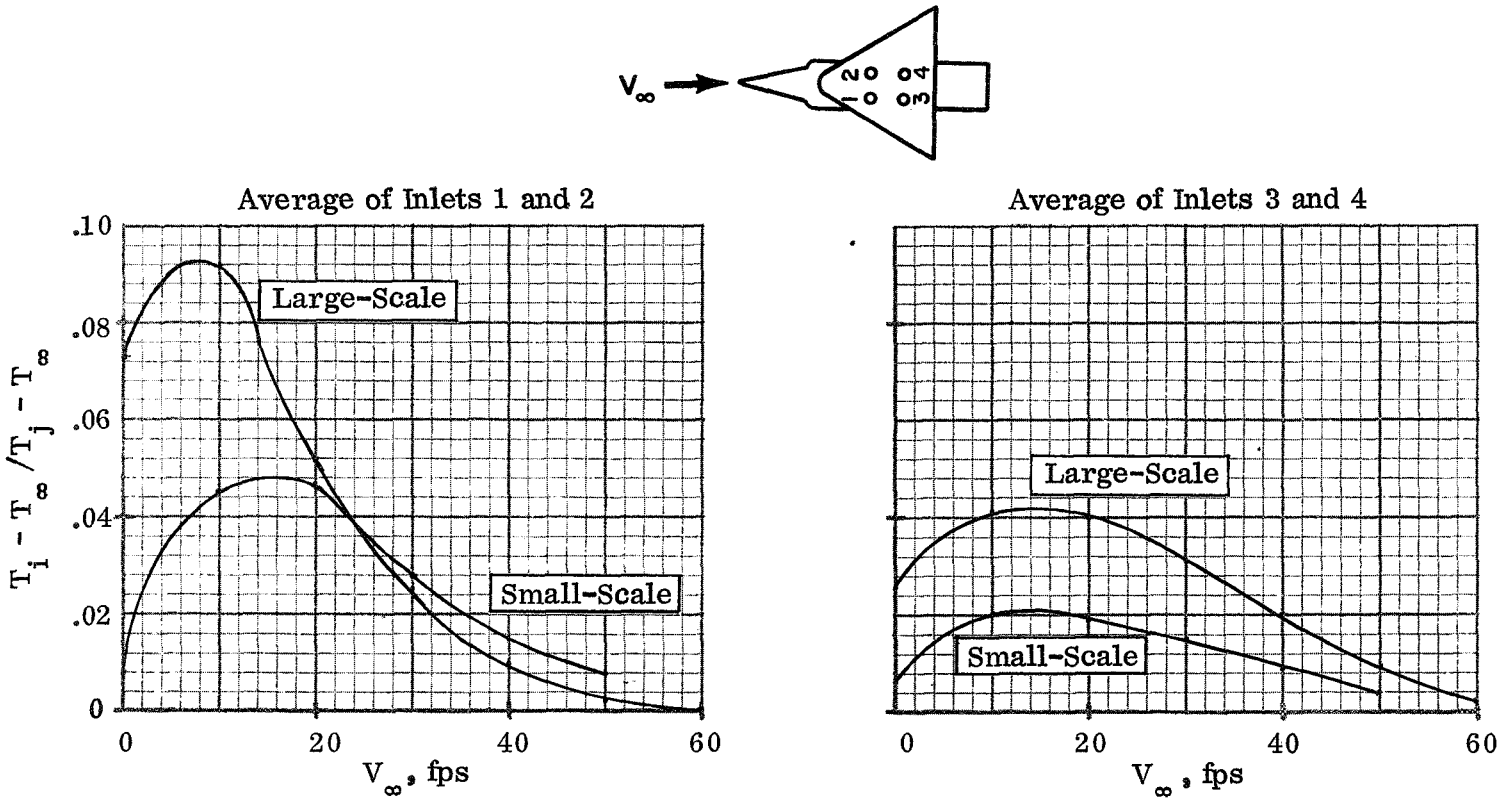


Figure 19. - Comparison of Small and Large-Scale ITR vs $V_\infty$ at Equal $V_j$ and $T_j$. Top Inlets Configuration, $\psi = 0°$

NASA CR-111867

DISTRIBUTION LIST
NAS1-10448

| | No. Copies |
|---|---|
| Lockheed-Georgia Company<br>86 South Cobb Drive<br>Marietta, GA 30060<br>Attention: Anthony E. Harris, Dept. 72-74, Zone 455 | 2 |
| Nielsen Engineering & Research, Inc.<br>3967 East Bayshore<br>Palo Alto, CA 94303<br>Attention: Jack N. Nielsen | 1 |
| Vanderbilt University<br>Department of Mechanical Engineering<br>Nashville, TN 37203<br>Attention: Professor J. W. Tatom, Box 11, Station B | 1 |
| Northrop Corporation<br>3901 West Broadway<br>Hawthorne, CA 90250<br>Attention: G. R. Hall, Internal Aero & Propulsive Branch<br>Organization 3711-31 | 2 |
| Dynasciences Corporation<br>Township Line Road<br>Blue Bell, PA 19422<br>Attention: E. Kisielowski, Director, Aero. Engineering | 3 |
| U. S. Army Aviation Materiel Laboratory<br>Fort Eustis, VA 23604<br>Attention: John White | 1 |
| Headquarters<br>Wright-Patterson Air Force Base, OH 45433<br>Attention: D. Hohler<br>G. Sealy<br>Lt. V. K. Smith III<br>C. Westbrook | <br><br>1<br>1<br>1<br>1 |
| Department of the Navy<br>Bureau of Weapons<br>Washington, DC 20525<br>Attention: Robert Brown, RAPP14 | 1 |
| Department of the Navy<br>Bureau of Ship<br>Washington, DC 20360<br>Attention: G. L. Graves | 1 |
| North American Aviation, Inc.<br>International Airport<br>Los Angeles, CA 90009<br>Attention: Rex Carpenter<br>Gordon Campbell | <br>1<br>1 |

NASA CR-111867

DISTRIBUTION LIST
NAS1-10448

| | No. Copies |
|---|---|
| Fairchild-Hiller<br>Republic Aviation Corporation<br>Farmingdale, Long Island, NY 11735 | |
| Attention: G. Rosenthal | 1 |
| J. Lyttle | 1 |
| Purdue University<br>Lafayette, IN 47907 | |
| Attention: Dr. J. C. Skifstad, Associate Professor<br>Mechanical Engineering | 1 |
| NASA Scientific and Technical Information Facility<br>P. O. Box 33<br>College Park, MD 20740 | 14 plus reproducible |